

POLITECNICO DI TORINO



Corso di Laurea Magistrale in
Ingegneria Energetica e Nucleare

PROCESS MODELLING OF A BIOGAS-FED
SOFC-ORC HYBRID SYSTEM

Relatori

Andrea Lanzini

Massimo Santarelli

Laureando

Alessandro Viola

Matricola: 208196

Anno accademico 2017/2018

Contents

Nomenclature table	2
Abstract	3
Introduction	4
1. Low power hybrid plants based on SOFC technology	7
1.1. SOFC-ORC hybrid systems	9
1.2. SOFC-Stirling hybrid systems	12
1.3. Trigeneration hybrid systems	15
2. Reference SOFC system	19
2.1. Base case: a 174 kW _{el} SOFC system fed with biogas from wastewater	19
2.1.1. The DEMOSOFC project	19
2.1.2. CONVION C50 solid oxide fuel cell modules	23
2.2. Opportunities for exhaust heat recovery	24
3. Assumptions and model development	26
3.1. SOFC model	28
3.2. ORC model	31
3.3. Aspen Plus® implementation	33
3.3.1. Base setup	34
3.3.2. Flowsheet definition and components configuration	36
3.3.3. Parameters' setup	44
4. Results	51
5. Conclusions	62
Table of figures and tables	64
References	66

Nomenclature table

R&D: Research and Development
RES: Renewable Energy Sources
SOFC: Solid Oxide Fuel Cell
WWTP: Waste Water Treatment Plant
HRU: Heat Recovery Unit
ODP: Ozone depletion Potential
GWP: Global Warming Potential
j: current density (A/cm^2)
V: voltage (V)
A: area (m^2)
T: temperature ($^{\circ}C$)
 U_f : utilization factor
D: diffusivity (cm^2/s)
M: molar mass (g/mol)
C-: Calculator
DS-: Design Spec
 \dot{m} : mass flow rate (kg/s)
 \dot{V} : volume flow rate (m^3/s)
 $(UA)_{tot}$: total heat transfer capacity (kW/K)
 ΔT_m : logarithmic mean temperature difference (K)
SP: Size Parameter (m)
 ΔH_s : isentropic enthalpy difference in the expander (kJ/kg)

Apices and Subscripts

ohm: ohmic
act: activation
conc: concentration
oa: anode exchange
as: anode-limiting
oc: cathode exchange
cs: cathode-limiting
FC: fuel cell
int: interconnector
e: electrolyte
a: anode, active
c: cathode
aeff: anode effective
an-ex: anode exit
cat-ex: cathode exit
cr: critical
f: factor
el: electric
wt: weight
rel: relative
is: isentropic
mec: mechanical
M: Motor
rec: recirculation
an.exh: anode exhaust
cnd: condenser
evp: evaporator
wf: working fluid
S4s: isentropic status at ORC expander outlet

Abstract

This work aims to develop a 0-D simulation model of a hybrid SOFC-ORC system and to estimate the benefits in terms of power production respect to the fuel cell alone. Reference case is an industrial Fuel Cell system with three modules. It is a Solid Oxide high temperature Fuel Cell working at atmospheric pressure, manufactured by the Finnish company Convion Ltd. It converts the chemical energy of a biogas flow from a Waste Water Treatment Plant into thermal and electric power up to 58 kW per module and releases gas exhausts at about 220°C.

Here it is supposed to use the latter for further power production by means of compatible power cycle. The low temperature gases as a source for the secondary cycle limit the choice within organic fluid cycle systems, absorption system, Stirling engines and the less known Kalina based systems.

Chapter 1 introduces in general terms the current R&D state of the art about hybrid systems based on SOFC technology. Some proposal and results from scientific papers are reported, so that the reader can have a comparison overview on the main features and the makings of hybrid plants.

In Chapter 2 the reference project is described and opportunities for waste heat recovery are discussed, starting from Fuel Cell datasheet. Also, the feeding flow composition is obtained from fuel sample data taken on the spot.

Reasoning about thermodynamic state of the exhausts available as heat source and the goal of this work ended in the choice of an ORC for further power production. So the assumptions behind the analysis development, as well as the equations for SOFC and ORC models, are reported in Chapter 3. There, also the most relevant features of the Aspen Plus® V8.0 software are described, together with the main steps of the entire simulation process.

The validation of the developed models and discussion of the results take place in Chapter 4, while conclusions are deduced in Chapter 5.

Introduction

Energy production relied on fossil sources for over a century, and the growing rate of economies in the latest decades made the climate change and health hazards two topics of strong interest.

This led to invest more in technology research for the exploitation of renewable energy sources, such as wind, sun, and more recently biomass, wastes, tidal energies, but also to improve the efficiency of consolidated conversion systems. The latter can guarantee lower rates of fossil sources consumption versus rapidly increasing amount of energy needing from emerging countries, during the period of transition to cleaner processes.

Fast facts

80%

of global energy consumption is based on fossil fuels

32.3 Gt

of global energy-related CO₂ emissions in 2014, unchanged from the preceding year. This marks the first time in 40 years in which there was a halt or reduction in emissions of the greenhouse gas that was not tied to an economic downturn

The representatives of developed countries met for the first time in Sweden in 1972 to talk about the protection, preservation, and the rationalization of human resources for the benefit of future generations...the concept of sustainable development was born!

However, the first step was actually taken in Kyoto in 1997, when 160 countries signed the obligation to reduce greenhouse gas emissions of 8.65% at least - respect to the values of 1985 - within 2012.

The agreement provided for:

- Modernization of industrial plants.
- Reduction of pollution from motor vehicles.
- Abolition of certain hazardous substances.
- Modification of chemical components used for refrigerants.
- Innovation in industries, especially in the energetic sector.

The Kyoto protocol entered in force in 2005, after Russia's signature (responsible for 17% of world emissions); Australia joined in 2007, and

Fig. 1: From International Energy Agency (IEA) website.

China and India too agreed, even if they are exempt from requirements on emissions. The USA never ratified the protocol, but they are now engaged in the program born from the 21st UNFCCC (United Nations Framework Convention on Climate Change), held in Paris at the end of 2015. There, 196 countries promised to accept binding commitments to prevent the temperature increase on the planet above 2°C within the period 2030-2050.

We could say this was a big step forward, nevertheless some choices strongly limit its effectiveness: 55 nations at least - source of 55% of global emissions as a whole - have to include it in their own legal system to get it started. Furthermore, the members themselves will decide their own goals, and no sanctions will be imposed if anyone will miss them.

However, without questioning the efforts of each one, these targets will undoubtedly slow down current trends of pollution increase, thus it is the good way.

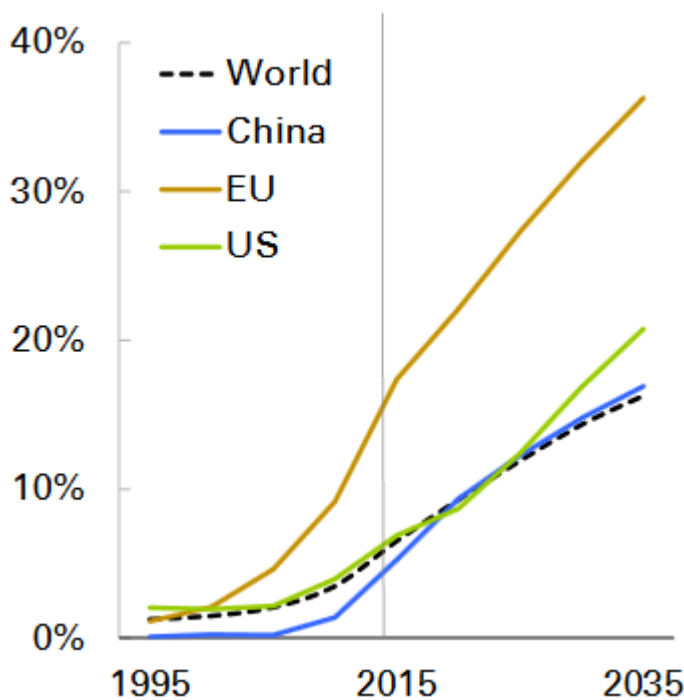


Fig. 2: Renewables share of power generation, from BP Energy Outlook (2016).

The European Union has always been at the forefront in supporting political efforts towards clean energy. Its leadership in renewable share of power generation (China will surpass everyone else in terms of volume growth by 2035) proves this. Renewables are expected to account for more than a third of EU power generation by 2035.

The EU itself covers less than half of its gross inland energy consumption (~46% in 2010) [1].

To increase its energy independence, combat climate change and strengthen its competitiveness, a set of goals by 2020 has been set: the 20-20-20 targets.

- Cut down greenhouse gas (GHG) emissions of at least **20%** below 1990 levels.

- Reach **20%** of EU's energy demand covered with renewable energy sources (RES).
- Improve energy efficiency in order to reduce primary energy use by **20%** with respect to 1990 levels [2].

To date RES cannot guarantee a continuous and reliable supply; furthermore, many related issues limit their spread, and probably the available area power density is one of the most influential. Thus, it is consistent to exploit existing plants by converting them to cogeneration and trigeneration, while carrying Research and Development (R&D) forward.

The EU has defined the financial tools (called "Framework Programmes") for research and technological development since 1983. During FP7 (2007 – 2013) about 4.65 bn€ were allocated to Non-Nuclear Energy (NNE) R&D, and they are increasing up to 5.4 bn€ within the Horizon 2020 programme [3].

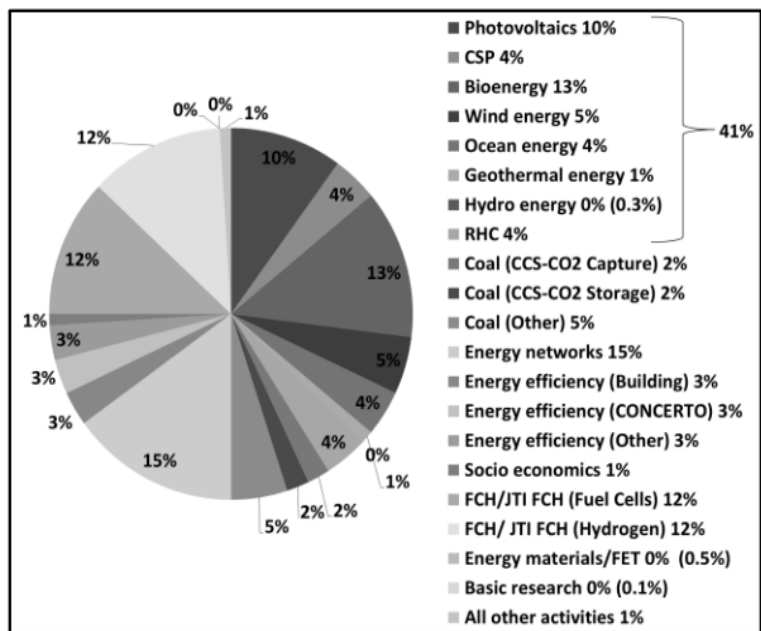


Fig. 3: FP7 funding for different NNE sectors.

Fig. 3: FP7 funding for different NNE sectors.

shows EU's interest in Fuel Cell technologies, as they joined a high amount of finance with more than 20% in FP7, and similar trends are for Horizon 2020 (2014 – 2020). This is of the utmost importance for such a promising low carbon technology, as the funding tools can help to lower its biggest drawback - i.e. costs – and accelerate its deployment.

1. Low power hybrid plants based on SOFC technology

Solid oxide fuel cells (SOFCs) have been considered as one of the most promising technologies for very high-efficiency electric energy generation from both natural and biogenous gas, and synthetic vectors too (H₂, synthetic NG, etc.). The high temperature exhaust gas from SOFC can be utilized in other cycles for additional power generation or for heating and cooling purpose (cogeneration/trigeneration). MCFC also can be used in hybrid cycle, but due to the cell reactions, the molten nature of the electrolyte and lower efficiency [4] vast majority of research in this field deals with SOFC combined cycles. There are some steady state [5, 6, 7, 8] and dynamic [9] modelling on the hybrid MCFC-GT cycles. However, the number of papers and diversity of such are not comparable with papers on SOFC hybrid cycle modelling.

The available papers show that the resulting maximum efficiency of SOFC-combined systems can be up to 90% [10] depending upon the operating condition and configuration used.

A significant research effort was spent on the design and optimization of SOFC/GT hybrid cycles, producing a large number of papers [11, 12, 13, 14, 15, 16, 17]. Conversely, experimental activities on SOFC/GT hybrid power systems are scarce, mainly due to the high capital cost required to build prototypes, even at a laboratory scale [18]. Probably, the most popular prototype is the 220 kW SOFC/ μ GT power system manufactured by Siemens Westinghouse and installed at the University of California [19]; a similar system, with an output of 300 kW, was also tested in Pittsburgh [20].

A certain number of researchers focused on the possibility to integrate SOFC, GT and Steam Turbine (ST) in a single combined cycle showing ultra-high efficiency [21].

Such opportunity was thoroughly investigated by Arsalis et al. [22], who analysed four configurations, in which the following differences regarding the steam turbine (ST) bottoming cycle were assumed: single pressure level, dual pressure level, triple pressure level with and without reheat. The purpose of using multiple pressure levels is to achieve a higher power output from the steam turbine. The SOFC stack is based on the internally reformed Siemens

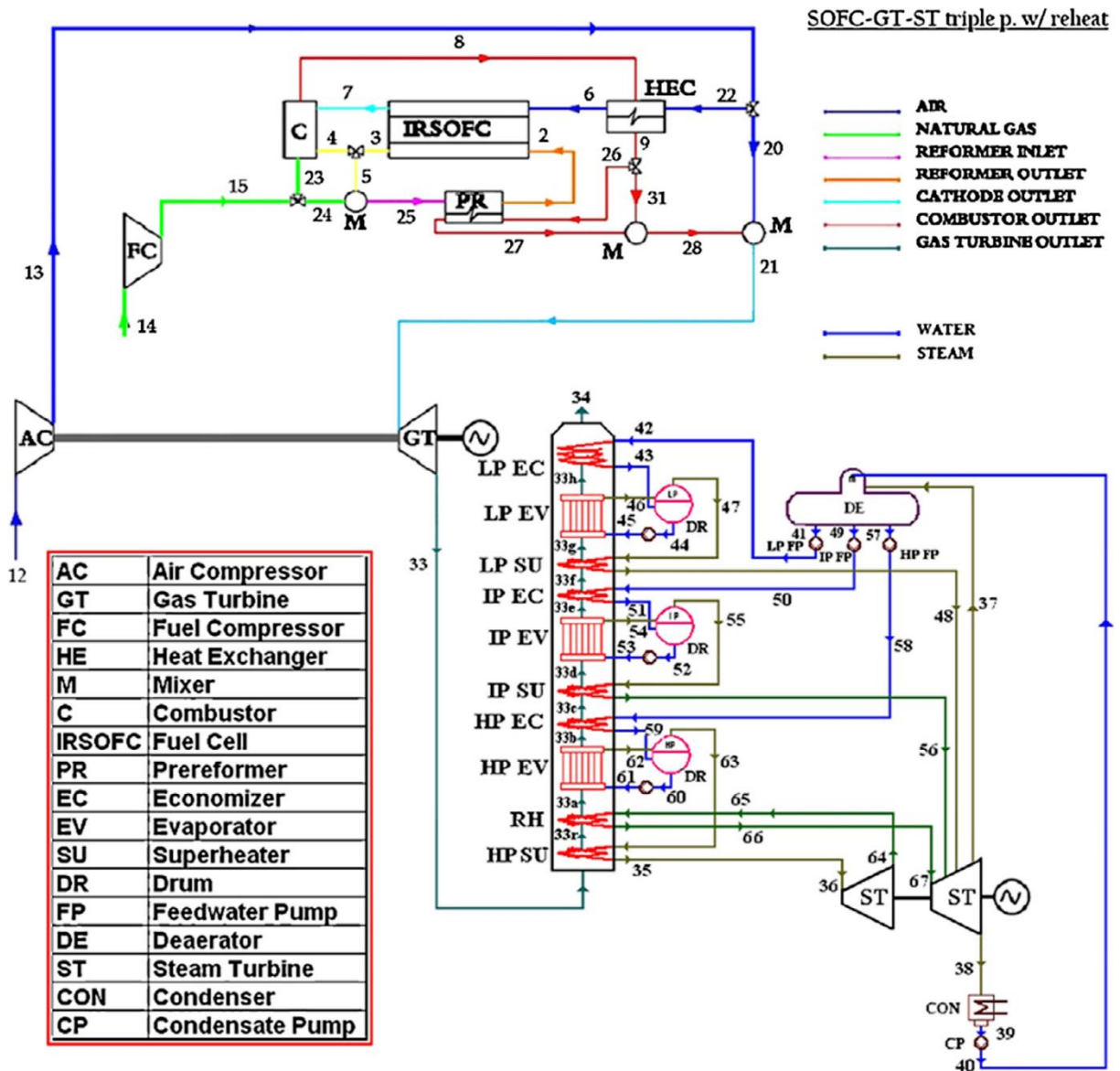


Fig. 4: SOFC-GT-ST combined cycle, studied from Alexandros Arsalis [22].

tubular configuration, equipped with a pre-reformer and an anode recirculation arrangement. Fig. 4 shows the layout of the hybrid SOFC-GT-ST power plant. The authors of this study considered three different hybrid plant sizes: 1.5MWe, 5MWe, and 10MWe. In addition, two different SOFC sizes are considered based on current density (from 100 mA/cm² to 650 mA/cm²). The systems were optimized varying the main synthesis/design parameters. Authors concluded that the hybrid SOFC-GT-ST configuration could be an excellent candidate for ultra-efficient power production. For instance, the 10MWe system with triple pressure and reheat exhibits a maximum efficiency of 73.7% and an average one of 65.3%. Furthermore, this hybrid power plant shows high efficiencies at off-design conditions as well. For a realistic system, a size of 1.5MWe is not as

Fig. 5 shows a generic layout for a SOFC-ORC combined system. The fuel cell here is fed with natural gas, so water must be integrated to let the steam reforming reaction happen. However, if the fuel were for example biogas from wastewater, the water line would have not been necessary.

The boiler before the exchangers for preheating is not always present, as it depends on design choices about the interfacing between the two cycles: the upper temperature of the ORC cycle could be so low that the heat from SOFC exhausts would be sufficient for both fuel-air-water preheat and bottom cycle supply. In fact the critical temperature range of usual working fluids goes from 100 to 400 Celsius degrees; to have a clear evidence of this, the temperature-entropy chart of a pair of “dry” fluids is shown in Fig. 6.

According to the same reasoning, the presence of the heat exchanger before the condenser is dependent on the lower temperature of the bottom cycle: if high enough, a further thermal process could exploit the remaining enthalpy, so that exchanger would make sense.

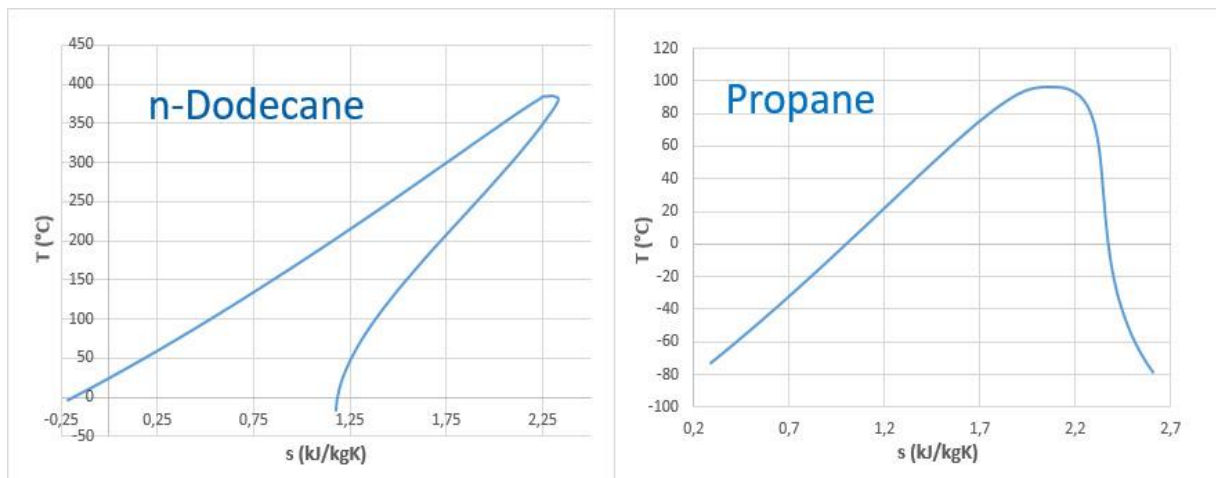


Fig. 6: T-s chart of n-Dodecane and Propane. Note the critical temperatures: next to 400°C and 100°C respectively.

Akkaya and Sahin [23] studied the energetic performance of a system that combined a SOFC with an ORC without any heating or cooling load. They found that the efficiency of the hybrid system increased by 14–25% compared to that consisting of SOFC only. They separately analysed the effects of ORC and SOFC parameters on the whole system, and chose the best compromise for each section. Turbine inlet pressure and condenser temperature were varied as ORC parameters (taking into account stability issues of the fluid and cost VS heat

transfer area for the condenser); current density, working pressure (so the compressor ratio), fuel utilization factor and cell temperature as SOFC variables.

Pierobon et al. [24] analysed a 100 kW hybrid SOFC-ORC power plant coupled with a gasification system. The plant is designed for a 0.5 km² cultivation area and it is fuelled by syngas obtained by woodchip gasification in a fixed bed gasifier. The combination of the gasification process with SOFC and ORC results in the plant configuration presented in Fig. 7. Wet woodchips with 33.2% moisture content (molar base) are supplied to the two-stage gasification plant for wood gas production. The cleaned wood gas is then preheated in a heat exchanger (AP; anode preheater) to 650°C before entering to the anode side of the SOFC stack, which is assumed to operate at 780°C. Unreacted SOFC fuel is burnt in an afterburner. Then, the off-gases from the burner are sent into an intermediate heat exchanger (IHE) where a diathermic oil supplies heat to the ORC subsystem. The ORC cycle is also equipped with an internal regenerator.

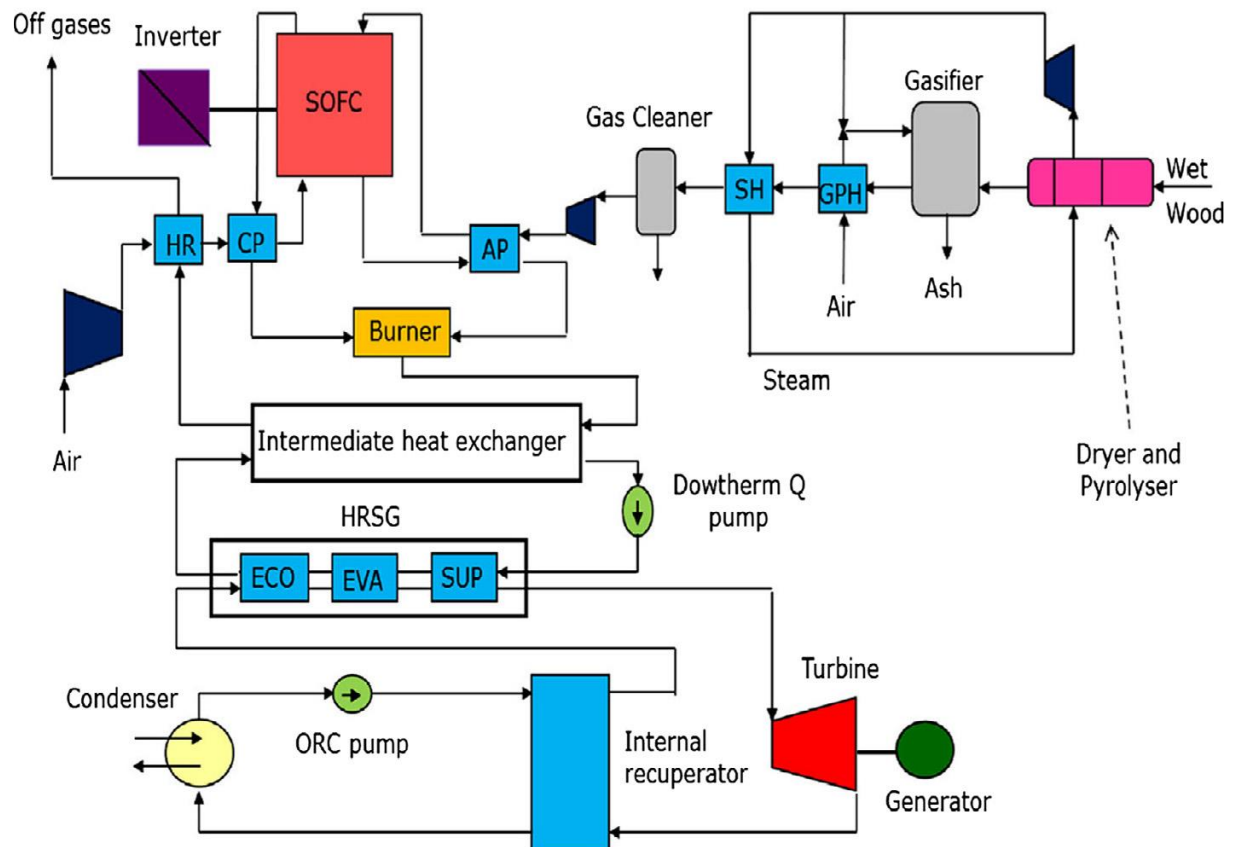


Fig. 7: Layout of a SOFC-ORC system powered by syngas [24].

Results of this study show that Gasification and ORC can potentially increase the system performance of 26.4%-points with respect to a conventional system.

In fact, simple and double stage ORCs fired by woodchips present a poor thermal efficiency (25.3% and 34.8%) compared to the IGSORC (56.4%). A maximum efficiency of 62.9% can be obtained by increasing the utilization factor of SOFC to 0.9 and decreasing its current density to 100 A/mm². Decreasing the operation temperature of the fuel cells to 650°C lowers the plant efficiency to 55.3%. Authors also performed a sensitivity analysis regarding the selection of the best working fluid for the ORC, showing that fluids with high critical temperature are required to achieve a high thermal efficiency. The results suggest that optimal fluid in terms of system performance is propyl-cyclohexane at 15.9 bar. When a limit at the outlet condenser pressure of 0.05 bar is imposed cyclohexane at 20.0 bar is the preferable working fluid.

Similar investigations are available in the literature, but they consider more complex systems, such as SOFC-ORC-adsorber for trigeneration or SOFC- μ GT-ORC to maximize electricity production. Thus, they will be mentioned below.

1.2. SOFC-Stirling hybrid systems

Stirling engines are volumetric machines in which a hot gaseous fluid performs a regenerative closed cycle. They are noted for being valve-less piston engines and quiet during operation. They are referred to as external combustion engines and often known as “hot air engines”, since air has been the designed working fluid for most of their history. By time, the deployment of new and resistant materials at lower costs led to the development of high-pressure engines. New fluids were required since performances would not appreciably increase with air. Moreover, higher pressures and temperatures carried the risk of fire of lubricants (air is an oxidiser), so helium, hydrogen and nitrogen began to be used.

Only a few studies have been carried out with a Stirling engine as a bottoming cycle when a fuel cell cycle is used as the topping cycle.

Masoud Rokni presents a small-scale SOFC-Stirling plant (10 kW) in Ref. [25]. Different configurations and fuels (Natural Gas, NG, ammonia, di-methyl ether (DME), methanol and ethanol) were analysed. The configuration with ammonia (Fig. 8) is the simplest one because the fuel can be directly fed to the SOFC cells, instead the one with NG is the most complex, requiring a desulfurizer and a pre-

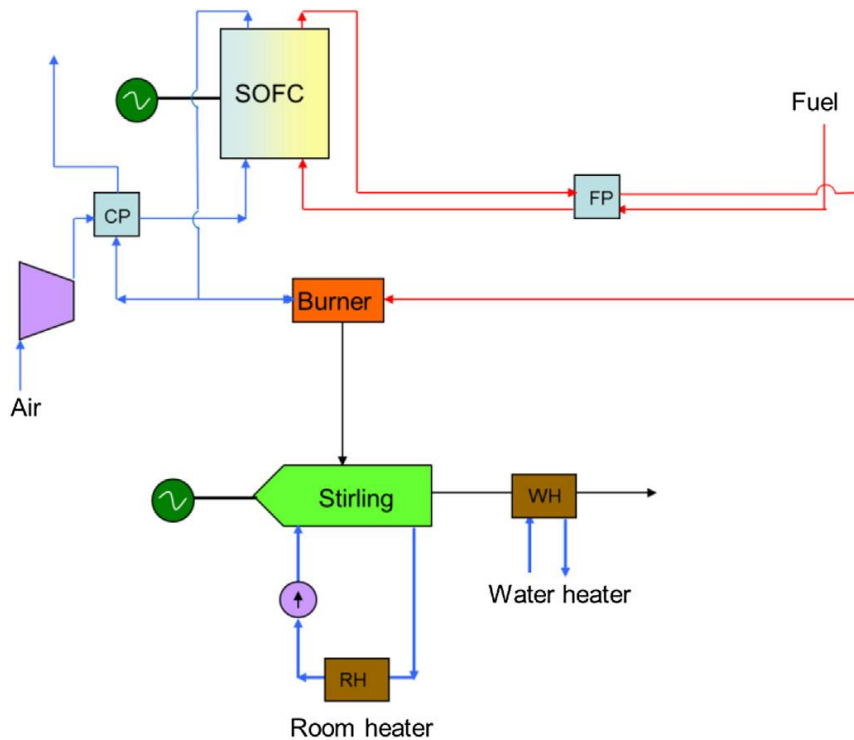


Fig. 8: A scheme of the combined SOFC-Stirling system fuelled by ammonia.

reformer reactor. The off-gases produced in the SOFC cycle feed a bottoming Stirling engine generate additional power. The off-gases and the cooling water of the Stirling engine are used to produce Domestic Hot Water (DHW) and space heating. For the combined SOFC and Stirling configuration, the overall power production was

increased by approximately 10% compared to that of a stand-alone SOFC plant. System efficiencies of approximately 60% are achieved, which is remarkable for such small plant sizes. There the results obtained let the author observe that with slight decrease in fuel utilization factor of the SOFC, fuel supply to the burner increases and the plant efficiency enhances regardless of fuel used since power produced from the bottom cycle of Stirling engine was found increasing (Fig. 9).

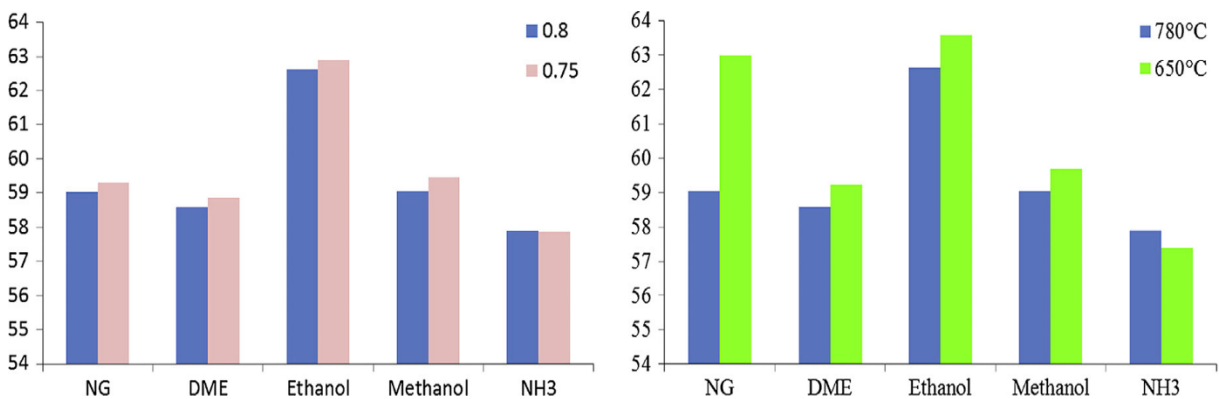


Fig. 9: The effect of the SOFC fuel utilization factor (left) and operating temperature (right) on plant efficiency [25].

Instead, by lowering SOFC operating temperature, the plant efficiency decreases for all fuels except for ammonia. The increase in plant efficiency was more pronounced with natural gas as a fuel.

The author also proposes the introduction of a methanator after the gas cleaning section to improve the CH₄ content in the fuel flowing to the anode. In that way a further, even slight, increase in efficiency is attained.

The latter improvement is theoretically confirmed again in Ref. [26, 27], where a small integrated gasification SOFC-Stirling plant is analysed: wood chips gasification in the first paper, Municipal Solid Waste (MSW) gasification in the second one. In both studies the net capacity is of 120 kW_e, which is suitable for use in decentralized CHP plants. Syngas is produced from wood chips gasification feedstock [26] and is utilized to feed directly the anode side of the SOFC stacks. Analysis shows that a thermal efficiency of 42.4% based on the lower heating value (LHV) can be achieved if all input parameters are selected conservatively. This value is relatively high if compared with existing large scale integrated gasification plants. The plant produces 127 kW of heat in terms of space heating and DHW. The electrical efficiency with the methanator increases, from about 40% to 42%, and of about 29% adding a Stirling engine at the SOFC plant. There is an optimal SOFC utilization factor, 65% (which is a rather small for SOFC), for which the plant efficiency is maximized (Fig. 10). This affects the amount of off-fuel available for the Stirling cycle. For lower values, more fuel will be for the Stirling engine, more power will be produced.

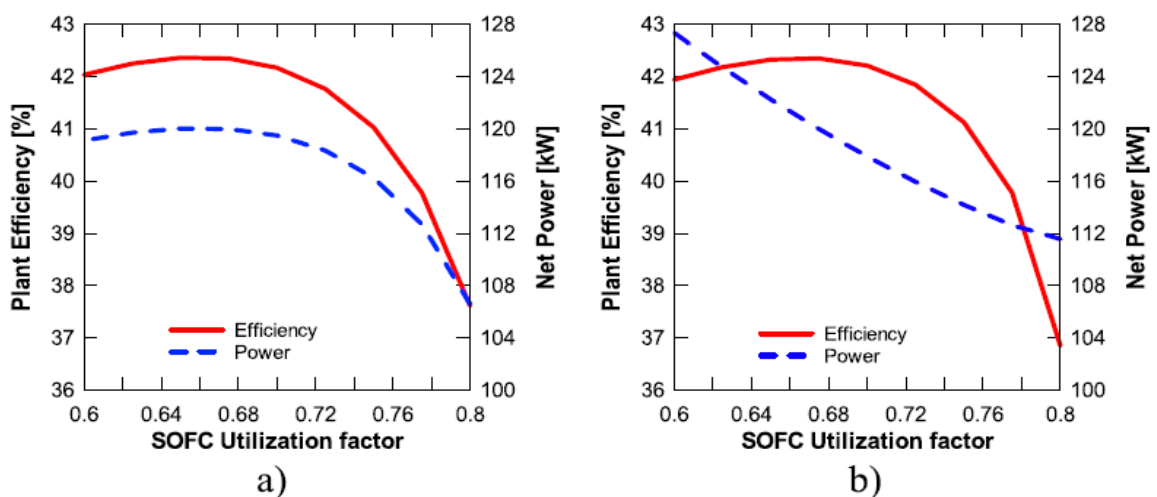


Fig. 10: Plant thermal efficiency and net power production as a function of woodchip mass: a) constant woodchip mass flow and b) constant SOFC electrical power [26].

Thus, the introduction of biomass gasification to the combined SOFC-Stirling hybrid systems decreases plant efficiency by more than 16%-points. This is aligned with other combined cycles when a gasifier is integrated to the plant. Such drop in electrical efficiency is not only the effect of integrated gasification but also depends on the nature (read quality) of the obtained syngas together with the type of gasifier.

Another “member” of the hot air engines family is the Ericsson engine, which actually is a special gas turbine engine where a reciprocating compressor replaces the turbocompressor and the turbine is replaced by a reciprocating piston/cylinder expander (Joule cycle reciprocating engine with external heat supply). The Ericsson configuration, with valves, shows several advantages compared to the Stirling configuration [28]. Amongst them, it is worth to note that the Ericsson engine heat exchangers are not dead volumes, whereas the Stirling engine heat exchangers designer has to face a difficult compromise between as large heat transfer areas as possible, but as small heat exchanger volumes as possible.

These features make the Ericsson engines deserve an interest equal to that to the Stirling engines. Even so, no studies on SOFC-Ericsson hybrid systems have been carried out.

1.3. Trigeneration hybrid systems

Trigeneration or combined heat, cooling and power production (CHCP) means the simultaneous production of mechanical power (electricity), heat and cooling from a single fuel. While CHP systems profit from more than 50 years of experience and are technologically well established, trigeneration is a quite recent technology and is becoming economically feasible thanks to the commercial spread of absorption chillers. Small-scale CHCP systems are an example of a novel concept in energy supply: DER, distributed/decentralized energy resources (for small-scale generation, likely below 1MW_e). The main potential in the service industry is in hospitals, hotels, sport centres, office buildings, shopping centres and district heating systems.

Ozcan and Dincer [29] presented a novel hybrid layout of a trigeneration system based on SOFC, ORC, solar collectors and an absorption chiller. The tri-generation system consists of: an internal reforming tubular type solid oxide fuel cell (IR-SOFC), which works at ambient pressure and fuelled with syngas; a combustor and an air heat exchanger; a heat recovery and steam generation unit (HRSG); a two-stage Organic Rankine Cycle (ORC) driven by exhaust gases of SOFC; parabolic trough solar collectors (PTSC); a lithium-bromide absorption chiller (AC) cycle driven by exhaust gases from SOFC unit. A scheme of the layout is shown in Fig. 11. The system is supplied by a syngas obtained by biomass gasification, consisting of 21% CH₄, 18% CO₂ and 40% H₂. The internal reforming SOFC stack is equipped with the anode recirculation arrangement in order to promote the steam reforming reactions. In addition, SOFC stack, consisting of tubular cells, is assumed to operate at ambient pressure. SOFC exhaust heat can be used to drive the absorption chiller and the ORC subsystem. The ORC operates using R245fa as fluid. ORC cycle is divided in two expansion stages in order to use solar heat for the low pressure turbine. In addition, solar heat is also used to preheat the organic fluid entering the HRSG. Finally, the heat rejected by the condenser is recuperated for residential water heating. Thermodynamic models, including mass, energy and exergy balances are implemented in order to calculate both energetic and exergetic analyses of the novel system. Results showed that the overall energy efficiency of the system is 85.1% and exergy efficiency is 32.62%. Highest irreversibilities occur in the SOFC unit and solar panels when considering sun as the heat source for panels. Tri-generation system energy efficiency and exergy efficiency are 52.5% and 13.4%, higher than that of SOFC stack energy and exergy efficiency. Solar collectors increase the overall system efficiency by 12–16% by providing an additional 89 kW of electricity production. Simultaneously, water heating and cooling energy are also provided. Finally, authors also performed a sensitivity analysis showing that system performance is dramatically affected by the appropriate selection of SOFC design parameters. An optimization may lead to a 5–8% system efficiency improvement [29].

A further analysis is presented by Al-Sulaiman et al. [30] investigating different arrangements of SOFC, ORC, solar collectors, biomass combustors and thermally driven chillers. Among the different layouts, authors also proposed the one

shown in Fig. 12. The system is based on a pressurized internally reformed SOFC stack where the steam required for the reforming process is supplied by an external heat exchanger. Biomass energy is used to preheat air and fuel entering

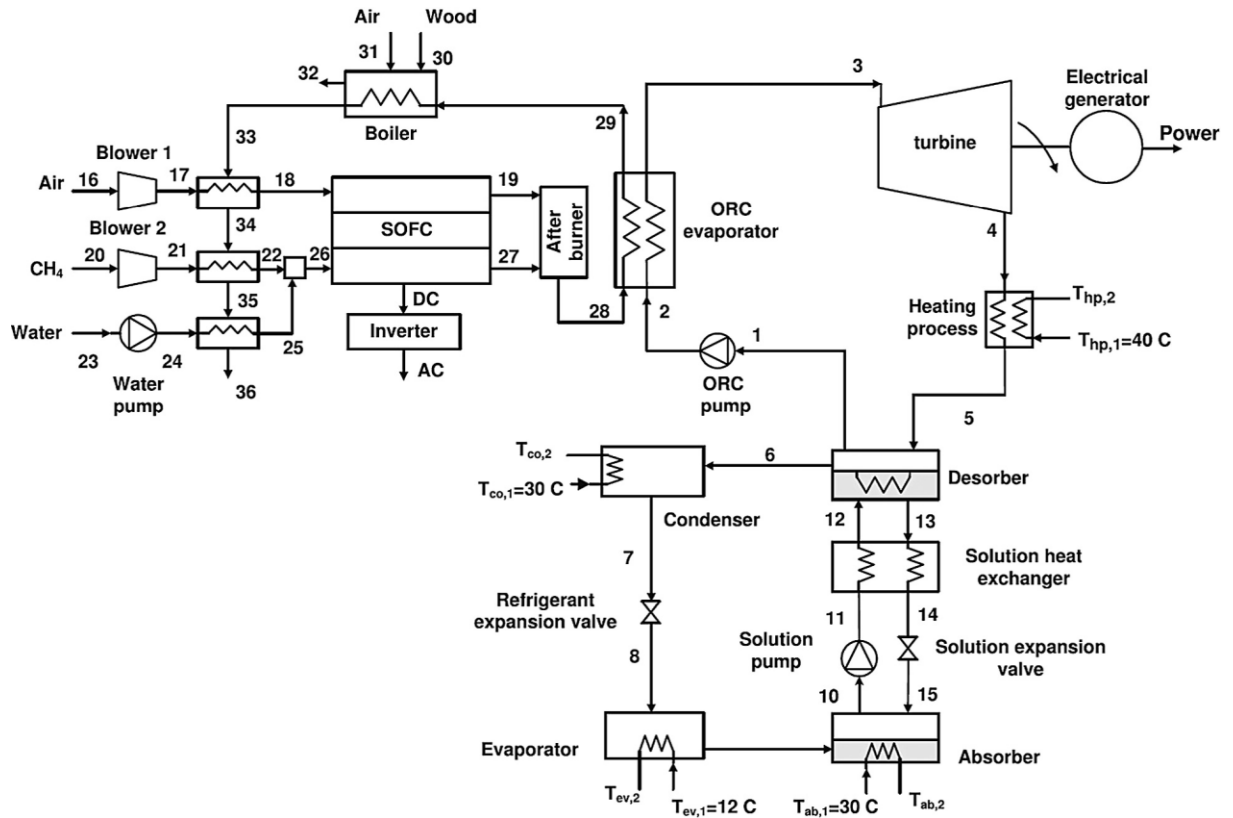


Fig. 12: SOFC-ORC-AC hybrid layout [30].

the stack and to produce the above mentioned steam. SOFC exhaust heat feed an ORC cycle. ORC rejected heat is partially used for heating process and partially to drive an absorption chiller, producing cooling energy. Authors performed several optimizations of the selected system, using a thermodynamic model of the components. They concluded that the electrical-exergy efficiency of the selected SOFC-ORC cycle is the highest among the considered systems. Conversely, the highest cost rate is achieved by the SOFC-trigeneration, due to the high capital cost of the SOFC subsystem, as well as the cost of the fuel for this system. Moreover, the cost per exergy unit of the SOFC-trigeneration system is the highest [30].

2. Reference SOFC system

In this chapter the analysed system will be described. The main subsystems are the fuel cell modules and the bottom cycle, which enhances the electric power output by converting the available heat from the SOFC exhausts.

2.1. Base case: a 174 kW_e SOFC system fed with biogas from wastewater

This paragraph introduces the reference system from which this work has been developed. It consists of three SOFC modules, which are fed with biogas and rated 58kW_e each one. The considered fuel is digester gas from anaerobic digestion of municipal wastewater.

The original project foresees the complete recover of exhaust gases from the cells to feed the digestion process, while this study considers the available heat as a source for a bottom cycle with further power production.

2.1.1. The DEMOSOFC project

The system is part of the DEMOSOFC project (**DEMO**nstration of large **SOFC** systems fed with biogas from WWTP), which aims to demonstrate how much helpful and reliable an innovative solution for distributed CHP generation based on SOFC technology could be to fulfil the European targets in the energy transition.

Its main objectives are:

- achievement of high performances of the integrated biogas SOFC system in terms of electrical efficiency, thermal recovery, low emissions, plant integration, economic interest for a better use of renewable fuels in a context of decreasing incentives to green technologies;

- management on the long run, maintenance experience, degradation issues: all in a real industrial context;
- exploitation and business analysis scenarios for the implementation of several integrated biogas SOFC plants across Europe;
- spreading of the higher energy and environmental performance of such systems and analysis of available market opportunities and for public awareness.

The proposed project is being installed in the SMAT wastewater treatment plant of Torino Collegno-Pianezza (IT) producing the biogas fuel.

The WWTP currently serves 270,000 equivalent inhabitants – a portion of the overall municipality of Torino – thus collecting an overall of 59,000 m³ of wastewater on a daily basis that corresponds to c.ca 220 litre/day/capita. Digester gas is available from the anaerobic fermentation of pre-thickened sludge at this facility. The suspended solid volatile (SSV) fraction in the sludge results in 1.34 wt. % leading to a biogas yield of 0.39 Nm³ of biogas per kg of SSV.

Given these site-specific productivity facts, and by taking the biogas-to-electricity efficiency of 53% (LHV basis) for the SOFC generator, the resulting electricity yield is about 1 W_e/capita.

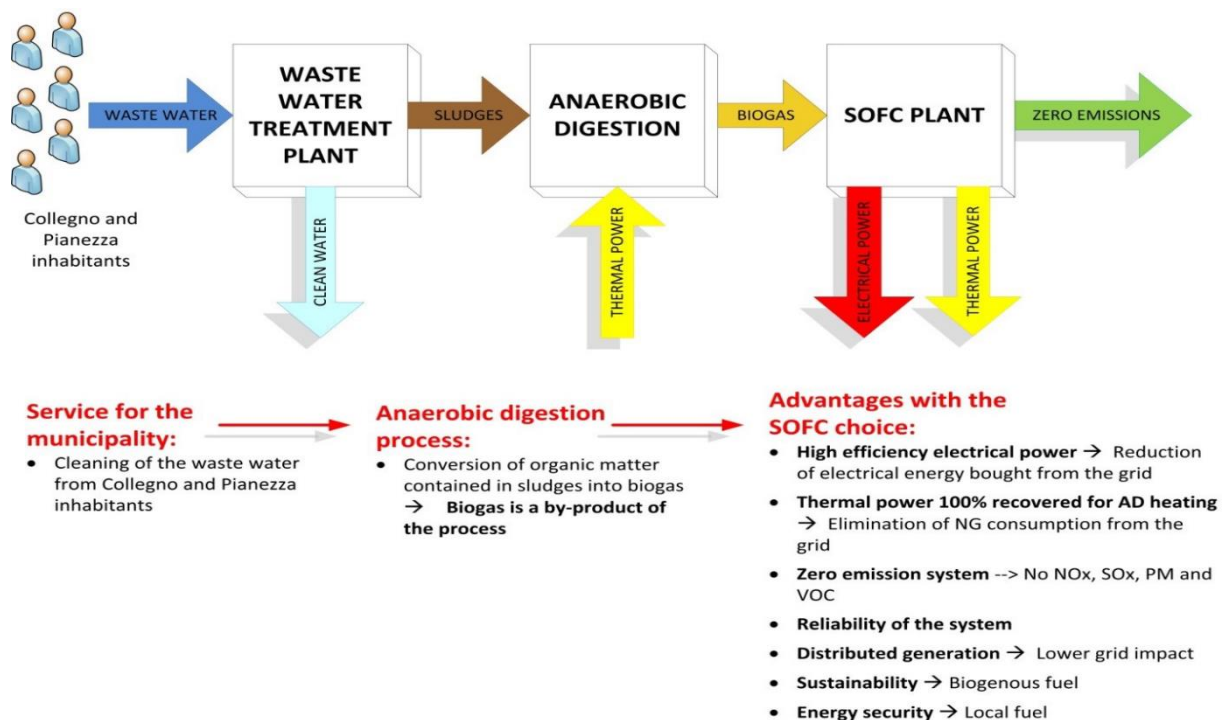


Fig. 13: Schematic flow diagram of Collegno WWTP after DEMOSOFC realization.

A distinctive feature of the integration of the SOFC within a WWTP is that both the electricity and heat produced are used onsite. Electricity consumption in the plant is generally higher than the electricity output from biogas as several pumps, compressors and other mechanical devices are in operation within the WWTP to process the wastewater. Looking instead at the thermal balance, the waste heat available from the SOFC can be almost fully recovered by pre-heating the sludge feeding the digester: this is a necessary step of the process, and the heat recovery from the SOFC allows the total substitution of external natural gas (fossil fuel consumption). Any surplus heat from the SOFC (generally available during the summer) could be exploited for other uses (e.g., domestic hot water in urban district heating loops).

According to some biogas samples taken in July, August and September 2015, the mixture composition was calculated. This was necessary since data were recorded for dry basis, while I was looking for wet composition to fill in the simulated fuel input.

Relative humidity is defined as the fraction of vapour mass with respect to the maximum possible value at which no condensation occurs. For ideal mixtures this is also the ratio of vapour pressure over saturation pressure at the same temperature:

$$UR = \frac{m_v}{m_{sat}(T)} = \frac{p_v \cdot V / (R_v \cdot T)}{p_s \cdot V / (R_v \cdot T)} \quad (1)$$

Relative humidity was reasonably supposed being 100% (digestion of urban wastewater), resulting that the vapour pressure was equal to that of saturated vapour; the mean temperature of the samples was of 33°C, while the flow pressure was just above the atmospheric one (c.ca 1.05 bar). Thus, according to the relationship for ideal gases:

$$\frac{n_{H_2O}}{n_{mix}} = \frac{p_{H_2O}}{p_{mix}} = \frac{p_s(33^\circ C)}{p_{mix}} = 4,74\% \frac{mol_{H_2O}}{mol_{mix}} \quad (2)$$

To recap, wet basis composition of biogenous fuel was computed from dry basis data, which were extrapolated from the analysis of samples taken at Collegno SMAT plant.

	Dry basis	Wet basis
CH ₄	64,10%	61,06%
CO ₂	31,53%	30,03%
O ₂	0,18%	0,17%
H ₂ O	-	4,74%
N ₂	4,19%	4,00%

Tab. 1: Biogas molar composition after digestion at Collegno SMAT plant.

The DEMOSOFC project includes a cleaning section for the removal of pollutants from the biogas. This is necessary to guarantee an acceptable lifetime of the cell, since mercaptans, siloxanes and aromatic hydrocarbons are present in the biogenous fuel. First design of the section is shown hereunder.

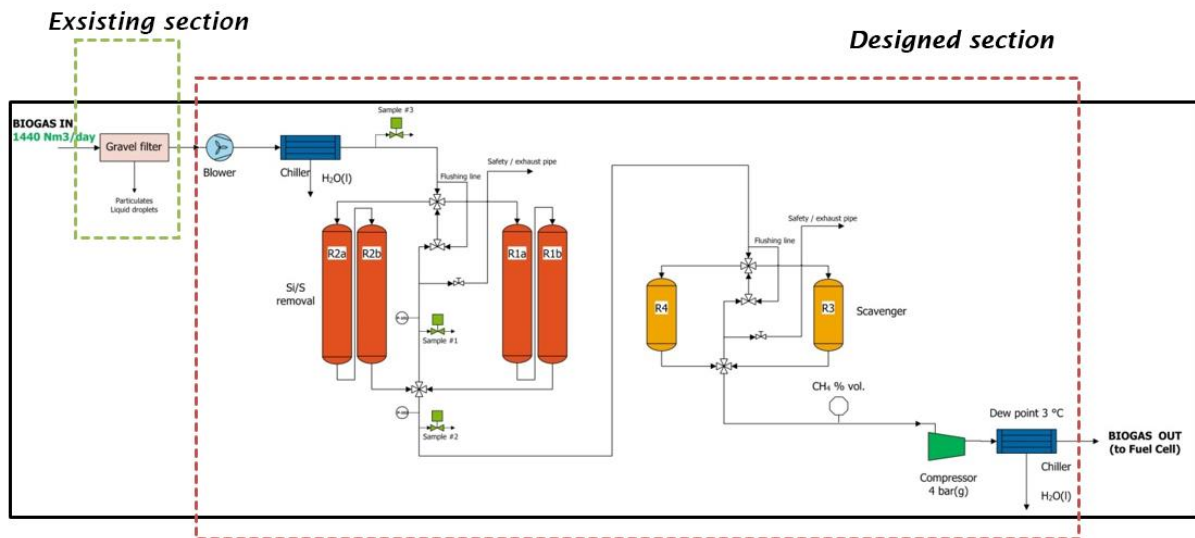


Fig. 14: Pre-treatment section for biogas cleaning.

2.1.2. CONVION C50 solid oxide fuel cell modules



Fig. 15: CONVION C50 Solid Oxide Fuel Cell module.

Convion C50 is a modular solid oxide fuel cell power generator with a nominal power output of 58kWe (AC Net). The product can be configured for operating with different fuel gas compositions and has a readiness for exhaust heat recovery. By its modular architecture, multiple C50 units can be installed in

parallel to achieve higher power outputs. Nevertheless, each module is a separate generator, able to operate autonomously. C50 is designed to be installed parallel to power grid but is capable of island mode, thus securing critical power loads within a micro grid. C50 is intended for continuous operation in a base load type generating mode. The units can be installed indoors or outdoors.

A standard C50 fuel cell unit consists of a nominally 58kW net stack module as well as process, automation and power conversion equipment for facilitating power generation from the unit. At the C50 module interface, pre-cleaned and pressurized fuel and clean, non-condensing pressurized air is required. Process air is taken in by C50 at ambient pressure. Inside of C50 system enclosure there is an interface for a recovery heat exchanger but the arrangement is not included in standard scope of delivery.

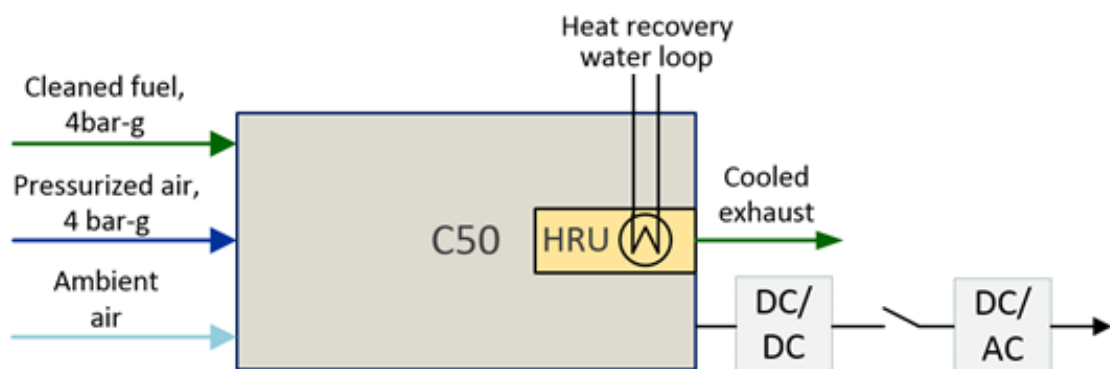


Fig. 16: Schematic of C50 interfaces.

Output of a single C50 module is summarized below in Tab. 2 .

Nominal AC Power [kW_e]	58
Electrical efficiency [% - LHV]	53
Electrical connection	3x400-440 V AC 50/60 Hz
Exhaust temperature @ rated power [$^{\circ}\text{C}$]	222
Exhaust flow rate @ rated power [kg/h]	650
Specific heat capacity of exhaust flow [$\text{J}/(\text{kg}\cdot\text{K})$]	1072

Tab. 2: Summary of typical C50 module outputs.

Unfortunately, further data and description of operation modes cannot be shared, since a Non-Disclosure Agreement (NDA) protects them.

2.2. Opportunities for exhaust heat recovery

It has been illustrated that working temperatures of Solid Oxide Fuel Cells are enough high to let them couple with any thermodynamic cycle. However, the development trends aim to lower the operating temperature in order to decrease the material costs while keeping performances. This, together with the sub-MW power standard in the overview of distributed energy districts, will make gas turbines and Rankine systems less attractive and beneficial over time as bottoming cycle. Micro gas turbines also are excluded, since they require an inlet temperature above 700°C to ensure acceptable efficiencies (see page 9).

The case here proposed comprehends a process plant that requires a considerable amount of heat. Moreover, the CONVION fuel cells produce off-gases at 220°C , so the most reasonable choice is that to recover the heat for the digester load. In fact, this is what the current DEMOSOFC project contemplates. In that case, a portion of the unconsumed biogas flow by the SOFC modules is necessarily sent to a boiler to compensate for the remaining heat demand.

Being the thermal source at 220°C even Stirling engines cannot work properly: they usually work with sources above $450\text{-}500^{\circ}\text{C}$ for acceptable efficiencies. There's only one case in which a 25kW Stirling prototype engine has been operated at 329°C . Cool Energy Inc. is the manufacturer and they claim it can operate in a low-temperature range ($150\text{-}400^{\circ}\text{C}$) [**Errore. L'origine riferimento non è stata trovata.**]. Also with ORC systems high efficiencies are observed with

fluids that operate with higher temperatures, nevertheless there is a wide availability of organic fluids having a critical temperature not far from 220°C.

This work does not aim to design a complex and dynamic system such as a Stirling engine, nor it wants to investigate relatively new technologies, such as Kalina systems (absorption systems where power is produced by expanding ammonia vapours in a turbine), thus the interest has been focused on ORC systems.

3. Assumptions and model development

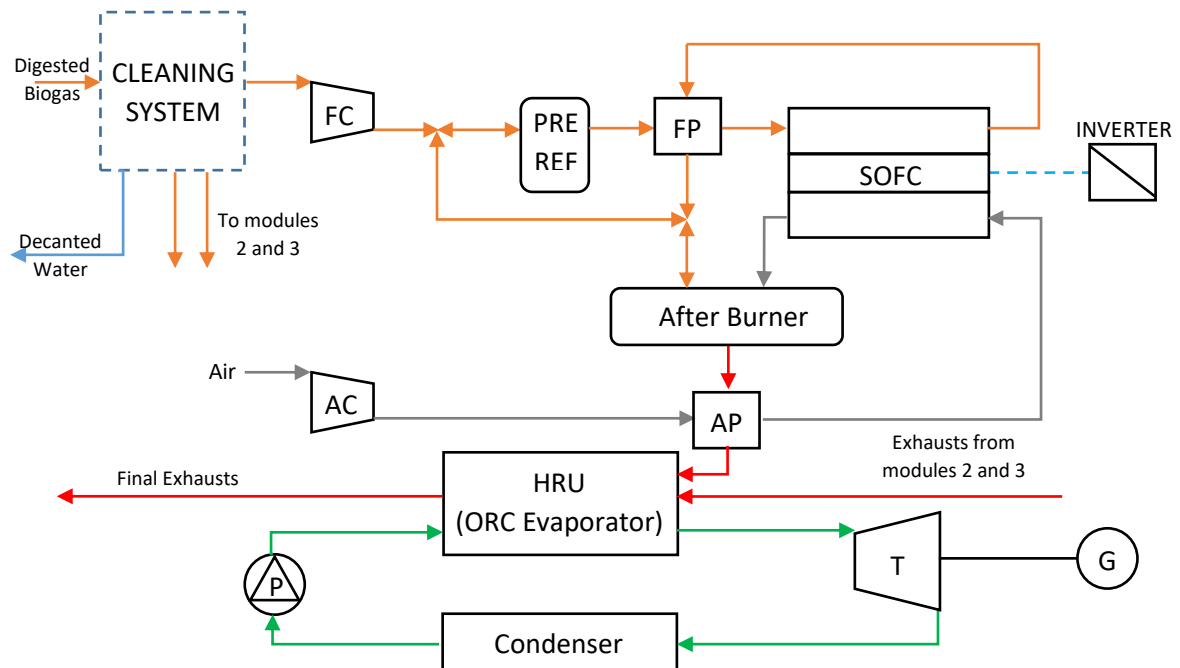


Fig. 17: Schematic diagram of studied SOFC-ORC system.

The studied system consists of three SOFC modules and an ORC cycle, as shown in Fig. 17 (for clearness purposes only one module is depicted). The waste heat from the SOFC is used to heat the organic fluid in the secondary system. Several assumptions were made to carry out the analysis. The ones for the SOFC are:

1. Air at the inlet of the SOFC consists of 79% N_2 and 21% O_2 .
2. Fuel cell operates at steady state and nearly atmospheric pressure.
3. Gas mixture at the exit of the fuel channel reaches chemical equilibrium.
4. Flow temperature at the inlet of the air and fuel channels of the SOFC is considered constant but not equivalent (cathode inlet is set almost $100^\circ C$ less than anode inlet).
5. The temperature inside the fuel cell is uniformly distributed (due to the implemented OD model, as described below).
6. Flow temperature at the outlet of the anode and cathode channels of the SOFC is considered constant and equivalent.
7. Radiation heat transfer between gas channels and solid structure is neglected.

8. Contact resistances are neglected, as well as pressure drops along the pipework.

Material composition and properties of CONVION C50 were unknown, and were assumed as Colpan et al. did [31].

Working temperature of the fuel cell (T_{FC})	850°C
Temperature difference between outlet and inlet (ΔT)	120°C
Exchange current density of anode (j_{oa})	0.65 A/cm ²
Exchange current density of cathode (j_{oc})	0.25 A/cm ²
Effective gaseous diffusivity through the anode (D_{aeff})	0.2 cm ² /s
Effective gaseous diffusivity through the cathode (D_{ceff})	0.05 cm ² /s
Thickness of anode (L_a)	0.5 mm
Thickness of cathode (L_c)	0.05 mm
Thickness of electrolyte (L_e)	0.01 mm
Thickness of the interconnect (L_{int})	3 mm

Tab. 3: SOFC input values that are fixed throughout the study.

The overall active surface area was not known a priori. In the end, the value of 20 m² was chosen, since it guarantees that the current density remains below 0.5 A/cm², as for the most of commercial cells.

A bottom cycle is a secondary system that exploits a (low-temperature) heat source available from the main system, so it is extra equipment whose addition is thermodynamically and economically justified by the improvements that it brings. Furthermore, here the exhaust gases from CONVION modules are at 220°C. For these reasons, this study considered an ORC system as simple as possible:

- Six working fluids have been taken into account in order to compare more than one result. Isentropic and lightly dry fluids have been chosen so that recovering of low de-superheating energy would not be worth the effort.
- Saturated steam is the Heat Recovery Unit (HRU from here on) output.
- Super-critical cycle is excluded to avoid strongly limiting properties concerning the choice of fluids.
- The condenser will be a gas/gas exchanger given that involved powers are low enough to require a relatively small surface. In this case, four values

of condensing temperature will be set in the simulation as mean values for all seasons.

The whole system has been simulated through Aspen Plus®. This software is being introduced in Par. 3.3.

3.1. SOFC model

The analysis of the SOFC model and efficiency equations are presented in this section.

The chemical and electrochemical reactions that occur within the anode and cathode of the solid oxide fuel cell are:



The cell voltage produced by the cell is the difference between the reversible cell voltage and the sum of the voltage loss. It is defined as:

$$V_{cell} = V_N - V_{losses} \quad (6)$$

where V_{cell} , V_N and V_{losses} are cell operating voltage, reversible cell voltage and voltage loss, respectively. The equation of the reversible cell voltage is derived using Nernst equation and is defined as:

$$\begin{aligned} E &= -\frac{\Delta\bar{g}^0(T, p^0)}{z \cdot F} + \frac{R \cdot T}{z \cdot F} \cdot \ln \left(\frac{\prod_{i=1}^{n_r} p_i^{\gamma_i}}{\prod_{j=1}^{n_p} p_j^{\gamma_j}} \right) = -\frac{\Delta\bar{g}(T, p)}{z \cdot F} = \\ &= -\frac{\sum_i n_i \bar{g}_i(T, p)}{n \cdot z \cdot F} = -\frac{\sum_i n_i \bar{g}_i(T, p)}{I} \end{aligned} \quad (7)$$

where:

- $\Delta\bar{g}(T, p)$ is the Gibbs free energy variation between reactants and products;
- z is the number of available electrons in the oxidation reaction;
- F is the Faraday constant (96,485 C/mol);

- R is the universal gas constant ($8.314 J/(mol \cdot K)$);
- T is the fuel cell temperature (that at which the reaction happens);
- p_i and p_j stand for partial pressure of reactants and products, respectively;
- γ_i and γ_j are the stoichiometric coefficients of the electrochemical reaction for the reactants and the products, respectively.

Given that Eq. (7) defines the highest possible voltage - open circuit condition - losses must be taken into account. These include the energies that the ionic and molecular transport mechanisms request, as well as the activation of reactions themselves:

$$V_{losses} = V_{ohm} + V_{act} + V_{conc} \quad (8)$$

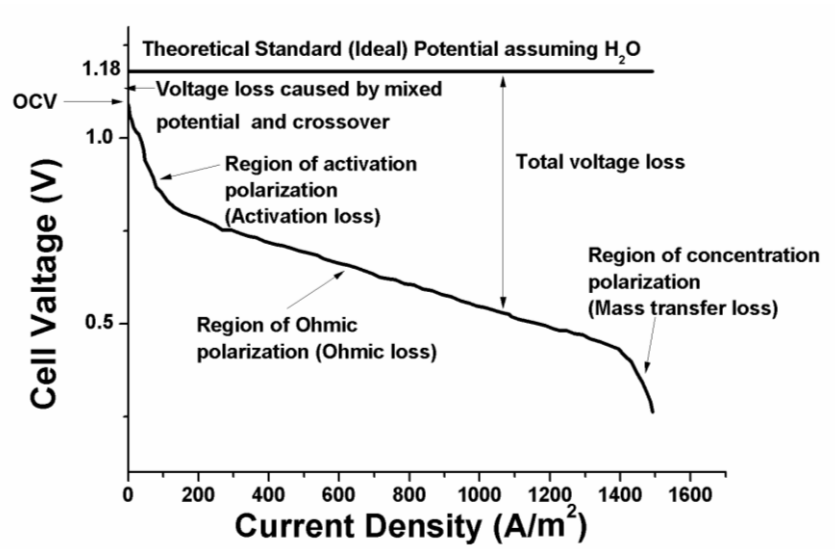


Fig. 18: Polarization curve of a fuel cell.

V_{ohm} is defined by Bossel [32]; V_{act} is defined by Kim et al. [33]; V_{cont} is defined by Chan et al. [34] as follows:

$$V_{ohm} = (R_{contact} + \rho_a \cdot L_a + \rho_c \cdot L_c + \rho_e \cdot L_e + \rho_{int} \cdot L_{int}) \cdot j \quad (9)$$

$$V_{act} = V_{act,a} + V_{act,c} \quad (10)$$

$$V_{act,a} = \frac{R \cdot T_{FC,exit}}{F} \left(\operatorname{asinh} \left(\frac{j}{2 \cdot j_{oa}} \right) \right) \quad (11)$$

$$V_{act,c} = \frac{R \cdot T_{FC,exit}}{F} \left(\operatorname{asinh} \left(\frac{j}{2 \cdot j_{oc}} \right) \right) \quad (12)$$

$$V_{cont} = V_{cont,a} + V_{cont,c} \quad (13)$$

$$V_{cont,a} = \frac{R \cdot T_{FC,exit}}{z \cdot F} \cdot \left(-\ln \left(1 - \frac{j}{j_{as}} \right) + \ln \left(1 + \frac{p_{H_2,an-ex}}{p_{H_2O,an-ex} \cdot j_{as}} \right) \right) \quad (14)$$

$$V_{cont,c} = -\frac{R \cdot T_{FC,exit}}{z \cdot F} \cdot \ln \left(1 - \frac{j}{j_{cs}} \right) \quad (15)$$

where

$$j_{as} = \frac{z \cdot F \cdot p_{H_2,an-ex} \cdot D_{aeff} / (R \cdot T_{FC,exit} \cdot L_a)}{10^6 [cm^3/m^3]} \quad (16)$$

$$j_{sc} = \frac{z \cdot F \cdot p_{O_2,cat-ex} \cdot D_{ceff} / \left(\left(\frac{p_{atm} - p_{O_2,cat-ex}}{p_{atm}} \right) \cdot R \cdot T_{FC,exit} \cdot L_c \right)}{10^6 [cm^3/m^3]} \quad (17)$$

where ρ and L are the electrical resistivity and the thickness of a cell component, respectively; $R_{contact}$ is the contact resistivity (hardly assessable, here will be neglected); j is the current density, j_{oa} and j_{oc} are the exchange current density of anode and cathode, respectively; D_{aeff} and D_{ceff} are the effective gaseous diffusivity through the anode and the cathode, respectively. For the meaning of the subscripts refer to the nomenclature table.

The electrical resistivity is defined according to Bossel equations_[32] for common SOFC materials:

$$\rho_e = (C1_e \cdot \exp(C2_e/T_{FC,exit}))^{-1} \quad (18)$$

$$\rho_a = (C1_a/T_{FC,exit} \cdot \exp(C2_a/T_{FC,exit}))^{-1} \quad (19)$$

$$\rho_c = (C1_c/T_{FC,exit} \cdot \exp(C2_c/T_{FC,exit}))^{-1} \quad (20)$$

$$\rho_{int} = (C1_{int}/T_{FC,exit} \cdot \exp(C2_{int}/T_{FC,exit}))^{-1} \quad (21)$$

Constants $C1_e - C2_{int}$ are defined in Tab. 4 below.

	C1	C2
Electrolyte	334	-10,300
Anode	$9.5 \cdot 10^5$	-1,150
Cathode	$4.2 \cdot 10^5$	-1,200
Interconnector	$9.3 \cdot 10^4$	-1,100

Tab. 4: Bossel constant parameters for common SOFC materials.

The current, the current density and the power of the fuel cell are defined respectively as:

$$I = j \cdot A_a \quad (22)$$

$$j = \frac{z \cdot F \cdot n_{H_2, in} \cdot U_f}{A_a} \quad (23)$$

$$W_{FC} = I \cdot V_{cell} \quad (24)$$

The net power produced is affected by the inverter system and by the auxiliary devices (mainly an air compressor), which are connected on the AC-grid side for safety reasons. Thus, recalling Fig. 16, we could define the net power and electrical efficiency as:

$$W_{net, SOFC} = W_{FC} \cdot 0,98 \cdot 0,96 - W_{AUX} \quad (25)$$

$$\eta_{el, SOFC} = \frac{W_{net, SOFC}}{\dot{n}_{fuel, in} \cdot LHV_{fuel}^{mol}} \quad (26)$$

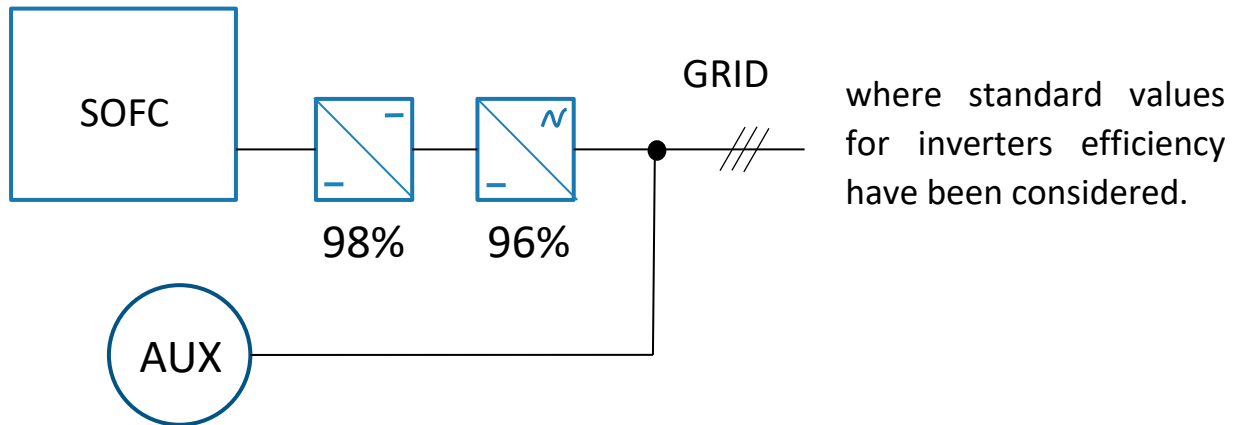


Fig. 19: SOFC unit-Grid interface.

3.2. ORC model

The type and physical properties of working organic fluids affect considerably the performance and cost of ORC. Therefore, it is important that the selected working fluid should meet some criteria. For example, it should provide efficient usage of the available heat source, low toxicity, good material compatibility, low cost, and low environmental impact.

A few organic fluids have been chosen among those with a critical temperature around the one of SOFC exhausts, i.e. 218°C. This was the base criterion for the selection. Secondly, other properties such as specific heat capacity, slope of saturation vapour curve, critical pressure, molecular weight, latent heat, toxicity, flammability and environmental impact have been considered.

- R141b (1-1-dichloro-1-fluoroethane, isentropic)
 $T_{cr} = 204.35^{\circ}\text{C}$; $c_p = 848.37 \text{ J/kg K @1bar, } 15^{\circ}\text{C}$; $P_{cr} = 42.1 \text{ bar}$
 $M = 116.95 \text{ g/mol}$ $ODP = 0.11$; $GWP = 725$
- R245fa (1,1,1,3,3-pentafluoropropane, isentropic), NON toxic
 $T_{cr} = 154.05^{\circ}\text{C}$; $c_p = 980.90 \text{ J/kg K @1bar, } 15^{\circ}\text{C}$; $P_{cr} = 36.4 \text{ bar}$
 $M = 134.05 \text{ g/mol}$ $ODP = 0$; $GWP = 1030$
- R123 (2,2-dichloro-1,1,1-trifluoroethane, isentropic)
 $T_{cr} = 183.68^{\circ}\text{C}$; $c_p = 738.51 \text{ J/kg K @1bar, } 15^{\circ}\text{C}$; $P_{cr} = 36.6 \text{ bar}$
 $M = 152.93 \text{ g/mol}$ $ODP = 0.02$; $GWP = 93$
- R600a (Isobutane, dry)
 $T_{cr} = 134.66^{\circ}\text{C}$; $c_p = 1981.42 \text{ J/kg K @1bar, } 15^{\circ}\text{C}$; $P_{cr} = 36.3 \text{ bar}$
 $M = 58.12 \text{ g/mol}$ $ODP = 0$; $GWP = 20$
- Toluene (Isentropic), flammable
 $T_{cr} = 318.6^{\circ}\text{C}$; $c_p = 1223.90 \text{ J/kg K @1bar, } 15^{\circ}\text{C}$; $P_{cr} = 41.3 \text{ bar}$
 $M = 92.14 \text{ g/mol}$ $ODP = 0$; $GWP = 3$
- R113 (1,1,2-Trichlorotrifluoroethane, isentropic)
 $T_{cr} = 214.2^{\circ}\text{C}$; $c_p = 886.5 \text{ J/kg K @1bar, } 15^{\circ}\text{C}$; $P_{cr} = 34.1 \text{ bar}$
 $M = 187.38 \text{ g/mol}$ $ODP = 0.9$; $GWP = 6000$

Mass and energy balances at steady-state conditions are performed by the simulation software internal engine, so the only equations to be specified remain the ORC power output and the Combined System (CS) efficiency.

$$W_{ORC} = (W_{Turb} \cdot \eta_T - W_{Pump}/\eta_P) \cdot \eta_G \quad (27)$$

$$W_{CS} = W_{net,SOFC} + W_{ORC} \quad (28)$$

$$\eta_{el,CS} = \frac{W_{CS}}{\dot{n}_{fuel,in} \cdot LHV_{fuel}^{mol}} \quad (29)$$

In order to insight and improve the performance of the proposed combined system, the effects of variation of main design parameters are investigated under wide range.

3.3. Aspen Plus® implementation

Aspen Plus® belongs to a well-known software suite developed by aspentech, aiding in simulating and analysing processes of chemical and manufacturing industry. The aforementioned code is oriented mainly on the chemical process optimization; in this work the 8th major release is used.

A system simulation in Aspen Plus® is structured into four main phases:

- **Simulation setup.** Chemical species and mathematical method for resolution are defined. Often non-mandatory entries are added, such as “property sets”, i.e. specific intensive or extensive physical magnitudes which are useful for subsequent analysis (some examples could be: dew point, specific heat capacity, chemical oxygen demand for a mixture, etc..).
- **Flowsheet definition.** The plant flowsheet is reproduced with all the needed components for its operation, even if some of the actual equipment may be “virtualized” with more than one among available ones in the code library. These are then linked together with mass and, eventually, heat/work flows.
- **Parameters’ setup.** Designed thermodynamic data are inserted into the model as input/output values for each component. Also, in this phase “Flowsheeting Options” are compiled. They allow to get to the designed process since the inputs alone are not sufficient to configure the whole system, being some or many variables interdependent. The “Design Specs” option allows to aim to a specific task without knowing a priori the right conditions: the designer chooses one or more parameters to be varied in a reasonable range in order to reach the target; “Calculator blocks” instead, are customizable Fortran/Excel sheets useful to calculate originated magnitudes, transfer parameters through the flowsheet, automating parameter refresher.

- **Computing and post-processing.** The code looks for any missing input and checks that no compatibility issue exists among given specifications (e.g.: pressure downstream of the turbine higher than upstream). Then it starts the simulation. This process is iterated until convergence is reached inside a tolerance window. It may end with warnings and errors too. The analysed results could eventually lead to a change in the configuration or in the setup. In addition, it is possible to define more than one sensitivity analysis, as well as optimization routines. This can be done through the “Model Analysis Tools”.

3.3.1. Base setup

The screenshot shows the 'Components - Specifications' window in Aspen Plus. The left sidebar contains a tree view with categories like 'Setup', 'Components', 'Molecular Structure', 'Assay/Blend', 'Light End Properties', 'Petro Characterization', 'Pseudocomponents', 'Component Attributes', 'Henry Comps', 'UNIFAC Groups', 'Polymers', 'Methods', 'Chemistry', 'Property Sets', and 'Data'. The main area displays a table of components with columns for Component ID, Type, Component name, and Alias. The table lists various chemical species, including hydrocarbons, gases, and solids.

Component ID	Type	Component name	Alias
CH4	Conventional	METHANE	CH4
CO2	Conventional	CARBON-DIOXIDE	CO2
O2	Conventional	OXYGEN	O2
CO	Conventional	CARBON-MONOXIDE	CO
H2O	Conventional	WATER	H2O
H2	Conventional	HYDROGEN	H2
H2S	Conventional	HYDROGEN-SULFIDE	H2S
N2	Conventional	NITROGEN	N2
C	Solid	CARBON-GRAPHITE	C
N2O	Conventional	NITROUS-OXIDE	N2O
NO	Conventional	NITRIC-OXIDE	NO
NO2	Conventional	NITROGEN-DIOXIDE	NO2
C2H6	Conventional	ETHANE	C2H6
CH2O	Conventional	FORMALDEHYDE	CH2O
R245FA	Conventional	1,1,1,3,3-PENTAFLUOROPROPANE	C3H3F5-D1
R141B	Conventional	1,1-DICHLORO-1-FLUOROETHANE	C2H3CL2F
R123	Conventional	1,1-DICHLORO-2,2,2-TRIFLUOROETHANE	C2HCL2F3-D1
R600A	Conventional	ISOBUTANE	C4H10-2
TOLUENE	Conventional	TOLUENE	C7H8
R113	Conventional	1,2,2-TRICHLORO-1,1,2-TRIFLUOROETHANE	C2CL3F3

Fig. 20: Component table defined in the Aspen code.

Defining involved chemical species was the first step. Biogas components, air and reaction by-products have been considered, plus the organic working fluid(s). Pollutants in the fuel have been neglected, since their total amount was less than 0,013%_{wt}. Moreover, the analysis is shaped around the energetic performances rather than the effects that pollutants could have on the materials of the cell. That said Fig. 20 shows the defined component table.

The chosen method for simulation solving was the one based on Peng-Robinson equation of state:

$$P = \frac{RT}{\tilde{V} - b} - \frac{a\alpha(T)}{\tilde{V}^2 + 2b\tilde{V} - b^2} \quad (30)$$

where:

$$a = 0.45724 \frac{R^2 T_{cr}^2}{P_{cr}} \quad (31)$$

$$b = 0.07780 \frac{RT_{cr}}{P_{cr}} \quad (32)$$

$$\alpha(T) = \left(1 + (0.37464 + 1.54226\omega - 0.26992\omega^2)(1 - \sqrt{T_r})\right)^2 \quad (33)$$

$$T_r = T/T_{cr} \quad (34)$$

with ω being the acentric factor.

This equation was developed in 1976 to satisfy the following requirements [35]:

- The parameters should have been expressed in terms of the critical properties and acentric factor;
- The model should have been reasonably accurate near critical point conditions, especially for compressibility factor and liquid density determination;
- Mixing rules should have used a single binary interaction parameter, the same being independent from temperature, pressure and composition;
- The equation should have been proper for all calculation of properties for fluids used in processes with natural gas.

Also, in order to have all the terms to fill the mathematical equations or just to monitor the reliability of results, some specific properties were added to those visible by default. They were:

- volumetric molar concentration of a component in a mixture;
- specific heat capacity of a mixture;
- dew point for a mixture;
- Gibbs free energy for a mixture;

- low heating value for a mixture;
- partial pressure of a component in a mixture;
- molecular weight for a mixture.

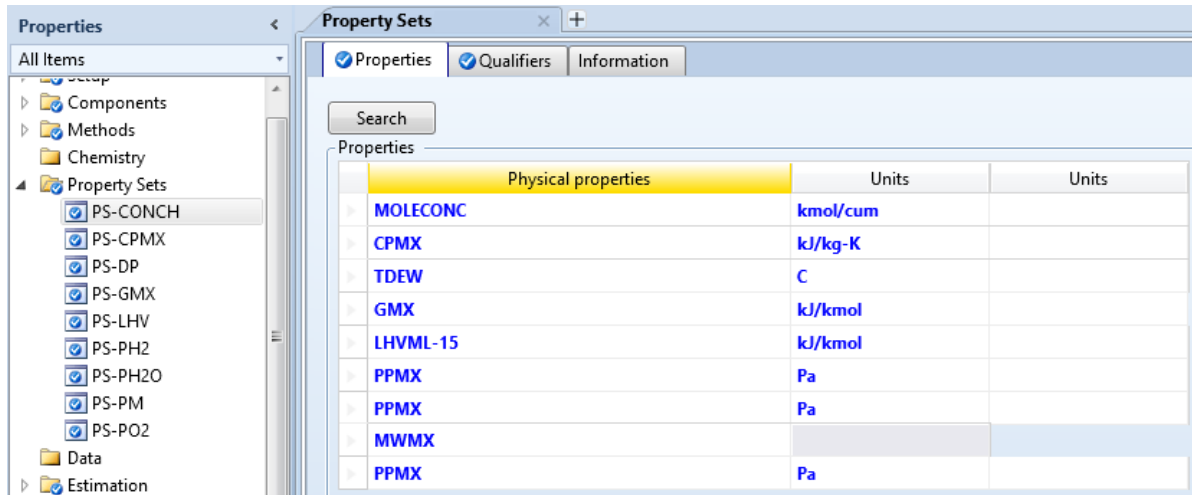


Fig. 21: Custom properties to be added in the streams results.

3.3.2. Flowsheet definition and components configuration

The interior layout of the CONVION cell cannot be shown here as it is covered by an NDA. The precise arrangement of the devices was not available anyway, so the simulation was conducted with assumptions of common sense. Fig. 22 in the next page shows the defined flowsheet which tries to reproduce the actual functional diagram.

As you can see symbolic items, connected together by lines, form the process scheme. The former are the stylized appearance of machinery and equipment, and they are called “blocks”; the latter, as it could be imagined, are mass streams of the working fluid. Dashed lines are for heat or work exchanges.

It is worth understanding how the electrodes have been reproduced here. Fuel cells basically are electrochemical reactors where electronic, ionic and mass transports are involved. The Aspen code contemplates the latest ones only, so a workaround was necessary to model the electrodes and compute the produced electric power.

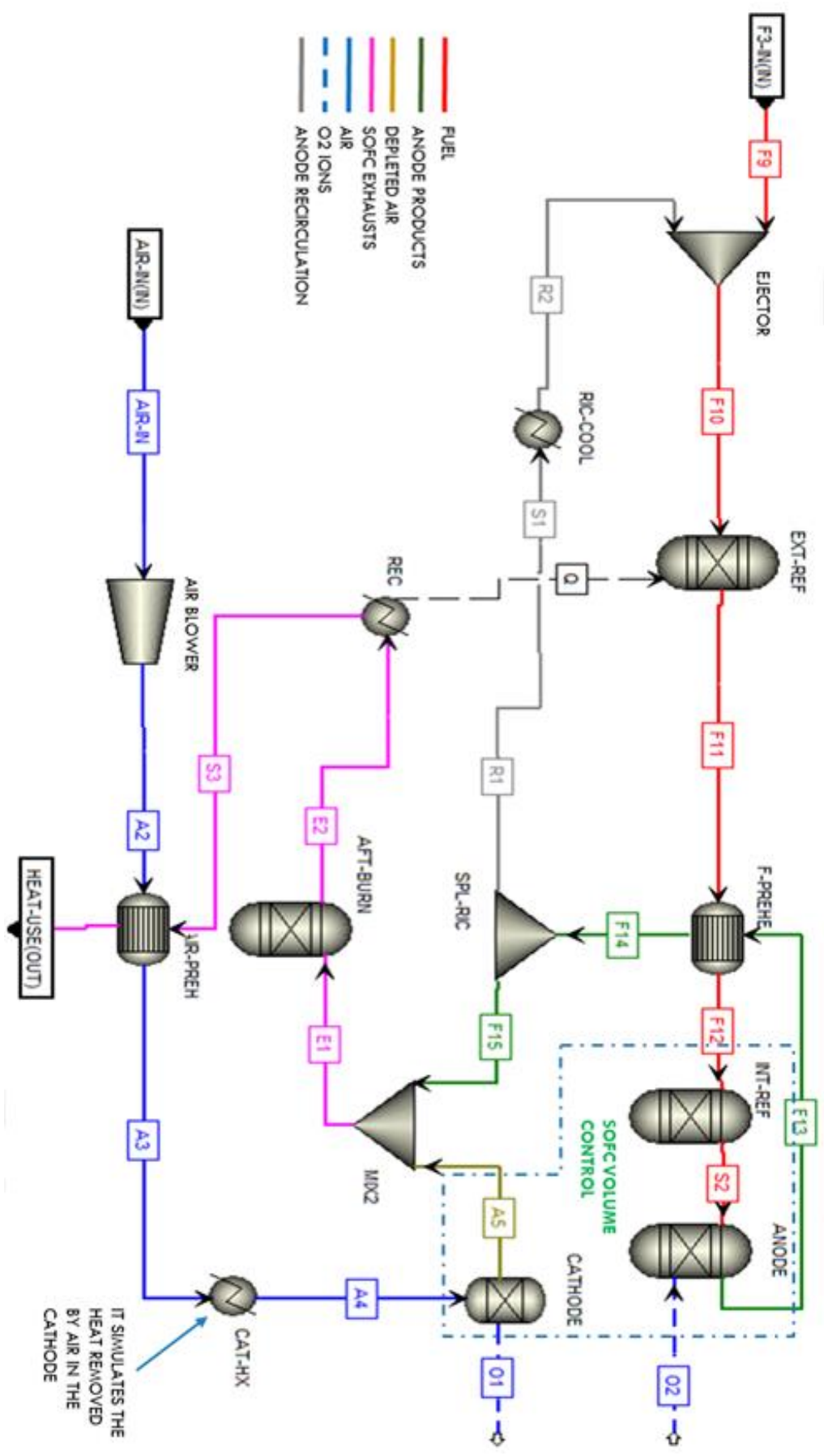


Fig. 22: Aspen Flowsheet for Convion CS0 module.

On top left (F3-IN) the biogas comes from the cleaning section (Fig. 14). This has been simulated too, in order to compute the actual fuel composition entering the fuel cell. As stated in Par. 3.3.1 the goal of this work does not comprise the analysis of the effects of pollutants on the cell, so the sulphur removal columns and the scavengers were simply seen as pressure drops. The two dew-chillers determined the values of the chemical composition, as they drain out condensed water. Recalling Tab. 1:

	Pre-Cleaning	Post-Cleaning
CH ₄	61.06%	67.30%
CO ₂	30.03%	28.60%
O ₂	0.17%	0.17%
H ₂ O	4.74%	0.14%
N ₂	4.00%	3.80%

Tab. 5: Comparison of the fuel composition downstream of the digester and upstream of the fuel cell.

The fuel enters the C50 module at about 4 bar_{rel}. This allows the use of an ejector as a recirculation “pump”. With no moving parts and less maintenance by using high-pressure fuel gas as the primary fluid to suck the anodic exhausts, anodic recirculation using ejectors increases the SOFC system reliability compared with other schemes. In fact, the high temperatures of the exhausts would require an expensive ATEX certified pump that is avoided with an ejector. The drawbacks are the cost for fuel compression, which can account for as high as 7% of the total cost of electricity. That is why an extreme care is usually taken in ejector design and operation for optimal system performance. In Aspen Plus there is not any block that works as an ejector, but it could be simply emulated with a “Mixer” block, whose outlet pressure is specified.

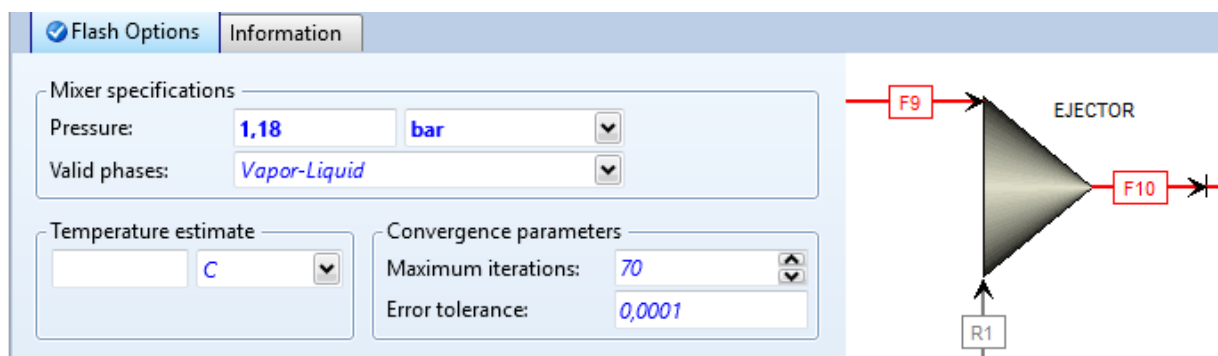


Fig. 23: A mixer block and its settings.

Next block is the “EXT(ernal)-REF(ormer)”, where steam reforming is realized. This reaction brings the advantage of removing heat from the core while guaranteeing a stable mixture in terms of carbon deposit at solid phase. That is also, why usually a pre-reforming is performed externally, so that the endothermic effect is not totally concentrated into the core and dangerous cold spots are avoided. On the opposite, the introduction of water in the anode lessens the partial pressure of active molecules, implying a negative Nernstian effect. The Aspen catalogue provides several reactor blocks, depending on the equilibrium approach the user prefers. For example, you would like to achieve chemical equilibrium based on stoichiometric approach, or you know the kinetics and you would use a plug flow reactor with rate-controlled reactions. Here a Gibbs reactor was chosen: it reaches a rigorous reaction and/or multiphase equilibrium based on the Gibbs free energy minimization. For this component it is mandatory to set the pressure: positive values refer to the outlet pressure while zero or negative values refer to the pressure drop (this is a general rule for this code). The second required input can be the heat duty – if known of course – or the outlet temperature.

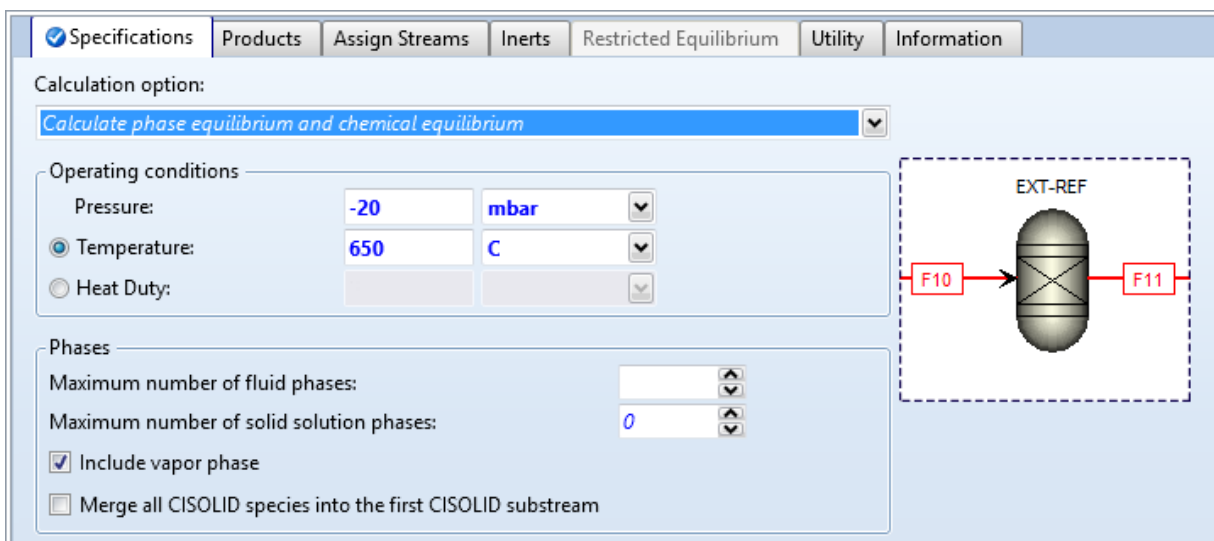


Fig. 24: Settings of the Gibbs reactor as the external reformer.

The steam reforming is observed from 612°C upwards, so a higher value must be set. As you can see in Eq. (3) this reaction requires water, so you would expect a water flow entering the reactor. However, here it is not necessary since a fraction of the cell exhausts is recirculated in order to provide water, and also to pre-heat the fuel. Since this reaction is endothermic, and a high temperature must be kept, it requires a high amount of heat. Usually a burner is set

downstream of the cell to exploit the remaining chemical energy of the exhausts, thus increasing the final temperature. The “Q” dashed stream is the heat recovered in the after-burner to support the steam reforming endothermic process.

Note that the “REC(uperator)” block is superfluous from a functional point of view. Nevertheless, the simulation software does not allow specifying how much of the total available heat has to be “re-routed” for a reactor. Thus, an external heat exchanger was the workaround to the matter.

Continuing with stream “F11”, the fuel is preheated and then enters the cell core. The “INT(ernal)-REF(ormer)” reactor represents the internal indirect reforming, whose heat is supplied by the core itself, while the “ANODE” block has an extra oxygen flow. The parameters to be specified are the same of those for “EXT-REF” block. Here the exothermal oxidation of the hydrogen into water occurs thanks to the oxygen coming from the cathode. So the electrochemical semi-reaction is virtually substituted by standard oxidation, given the reasons stated before.

On the other side an air blower sucks in the air and pushes it through a pre-heater in order to avoid thermal shocks to the electrode (having the same task of the fuel pre-heater). In Fig. 25 you can see what you can define for compressor blocks.

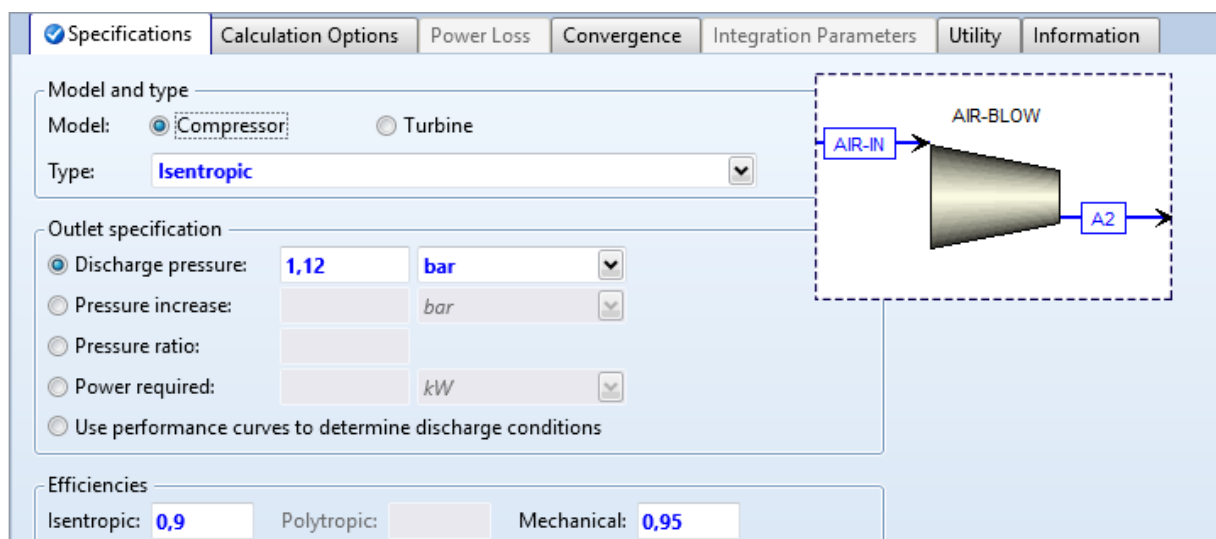


Fig. 25: Settings for the air blower (single stadium compressor).

The air is preheated to about 120°C below the fuel cell temperature by the exhaust gases.

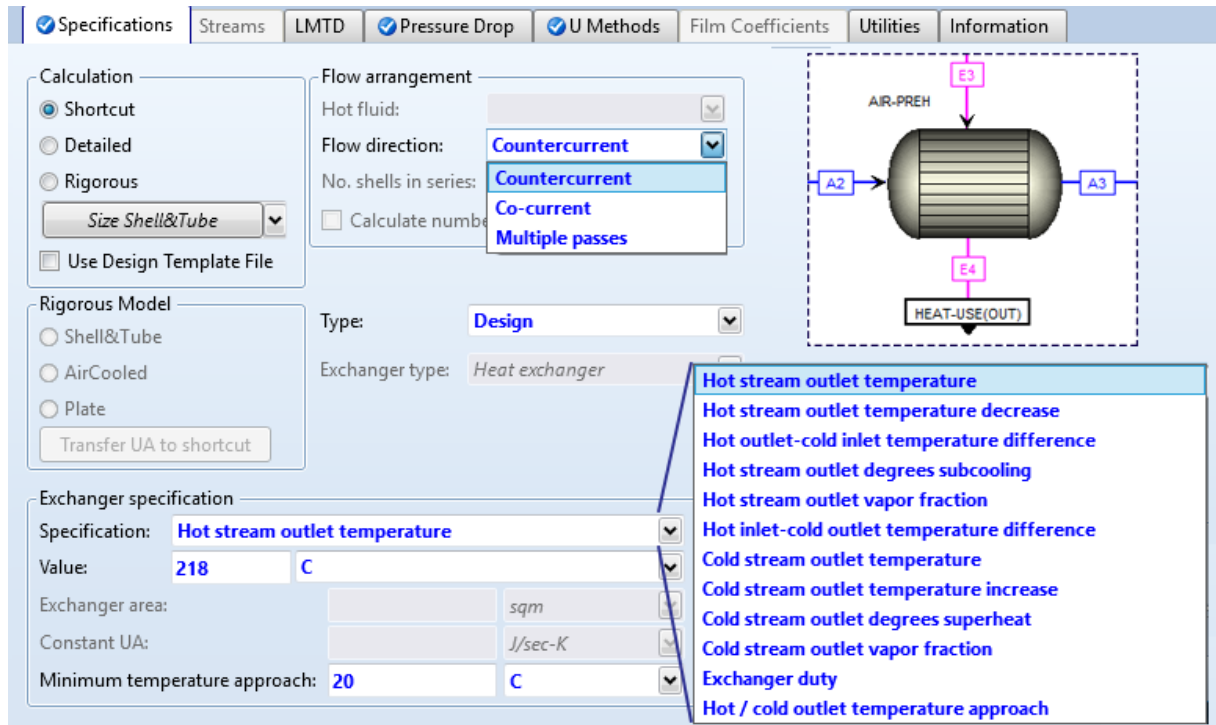


Fig. 26: Available settings for a two-stream heat exchanger block.

In this regard, a shell and tube counter flow exchanger was chosen, with the known hot stream temperature as output. Also, a reasonable (maybe even conservative) pinch point approach of 20°C was set.

The core of the whole model implementation - i.e. the “place” where the Aspen code sees the energy production – is the anode reactor. From this point of view, a cathode reactor would have no meaning, since the hydrogen oxidation to

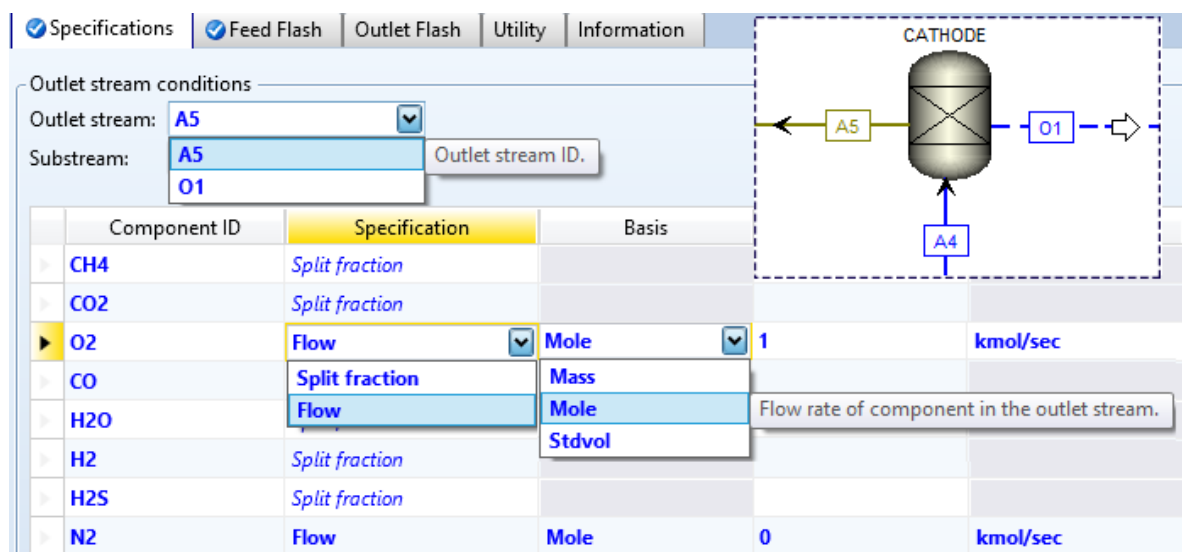


Fig. 27: Setting of the separator emulating the cathode. Oxygen only proceeds into stream O1 (O²⁻ ions).

water is considered as a direct reaction in the anode. Thus, a separator block emulates the reduction semi-reaction in the cathode, and sends a pure oxygen flow to the anode. You can set the desired conditions for either one or every outlet stream of this block, based on split fraction as well as on molar flow (see Fig. 27). Actually, the electrolyte is ignored with this approach, even if this configuration implies the simulation of an anionic electrolyte.

However, we must consider that the air flow is also necessary to cool the core, other than supplying oxidant to the reaction. The separator does not allow heat duty computation, so an additional heat exchanger is needed immediately before it (its usefulness is being clarified in the next paragraph). You can specify the outlet temperature or the heat duty for this type of block. In the first case the code will show how much heat you must supply or you could recover (with higher or lower temperature, respectively) as soon as simulation will run; in the second one the outlet temperature will be computed: higher with a positive duty or lower with a negative one.

By selecting “Degrees of superheating/subcooling”, the second field is limited to pressure properties for obvious reasons.

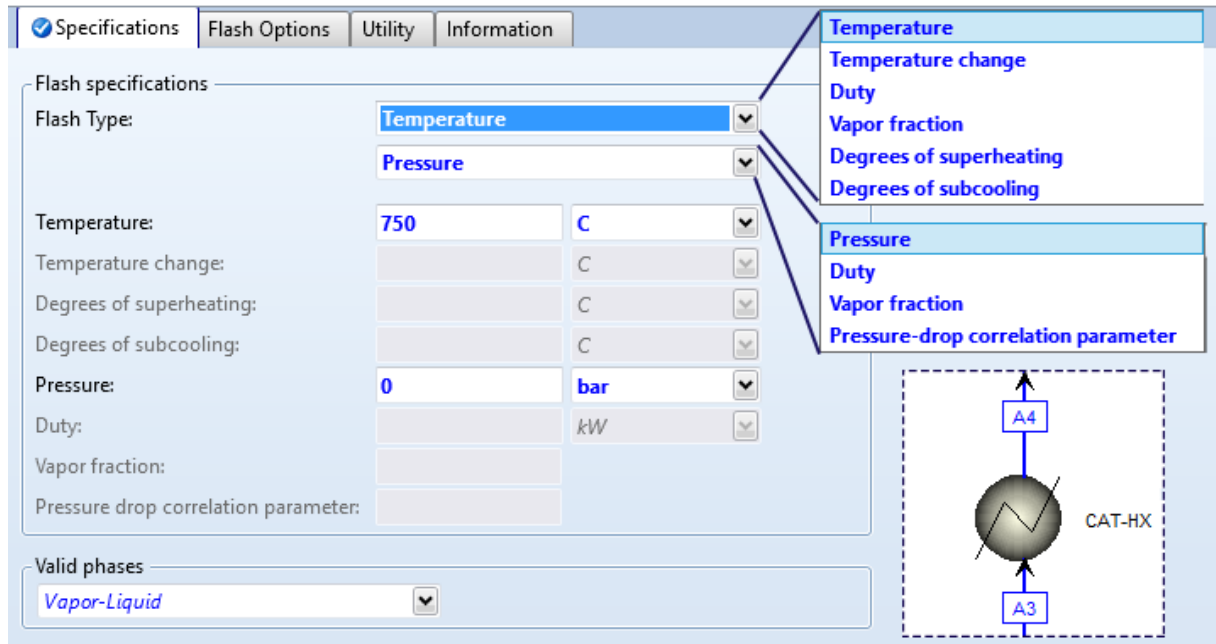


Fig. 28: Simple heat exchanger block. It helps in accounting for the right amount of cooling air.

A condition on the “Steam to Carbon ratio” (SC) was set as a rule to control the recirculation branch.

The rest of the exhaust gases is burnt with depleted air (the cooling air from cathode) in an afterburner in order to feed heat in the external reformer. Here the assumption of adiabatic combustion was made, so a null heat duty was set for the last Gibbs reactor.

Thanks to their high temperature, the exhausts can also preheat the air flow and escape the cell module at about 220°C. Then they are collected from the three modules and exploited as a heat source for a bottom cycle.

The ORC system consists only of basic components: the organic fluid is compressed by a pump and sent into the HRU, where it partially recovers thermal power from the CONVION modules' waste heat. At saturated vapour condition it enters the turbine and expands till condensing pressure (plus pressure drops of course). The simulation foresees different temperature values of condensation, likely the four main reference values along the yearly variation. Thus, by considering a minimum temperature difference of 10°C at the evaporator, the analysis has been performed for 15, 25, 35 and 45°C condensation temperature.

The ORC flowsheet is presented in Fig. 29:

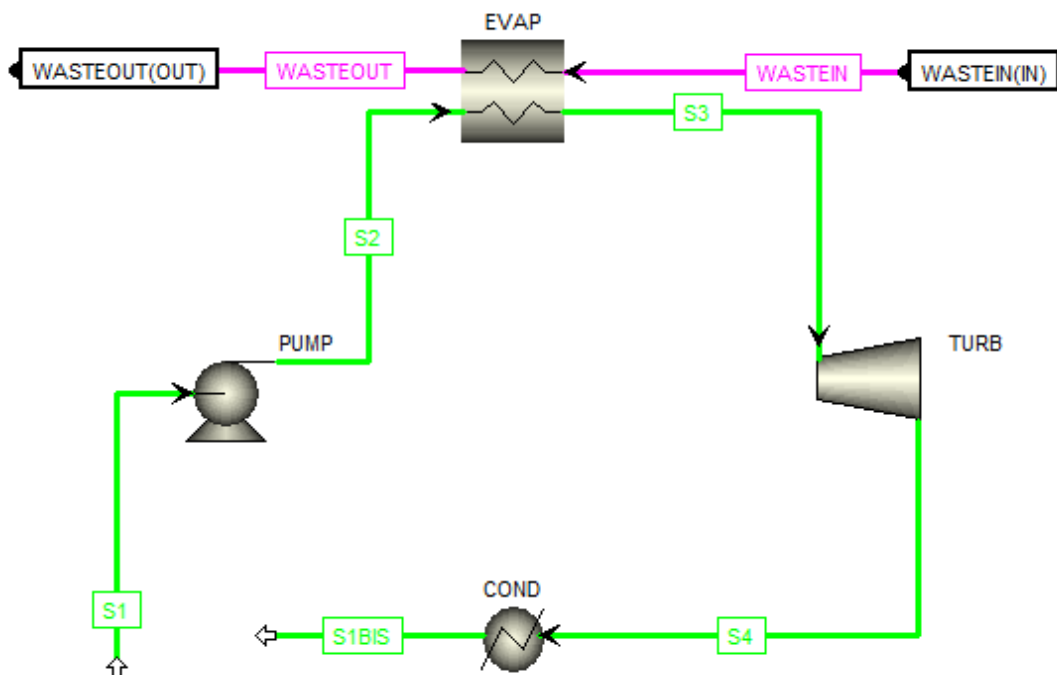


Fig. 29: Flowsheet of the Organic Rankine Cycle section of the system.

Pump and Turbine components allow the same settings of compressor (Fig. 25): other than the template picture, they are under the same category in the model

palette.

EVAP component is a multi-stream heat exchanger that can perform zone analysis if needed. Unlike the two-stream heat exchanger Fig. 26, it allows to specify heat leakage by fraction, and not through the global thermal coefficient.

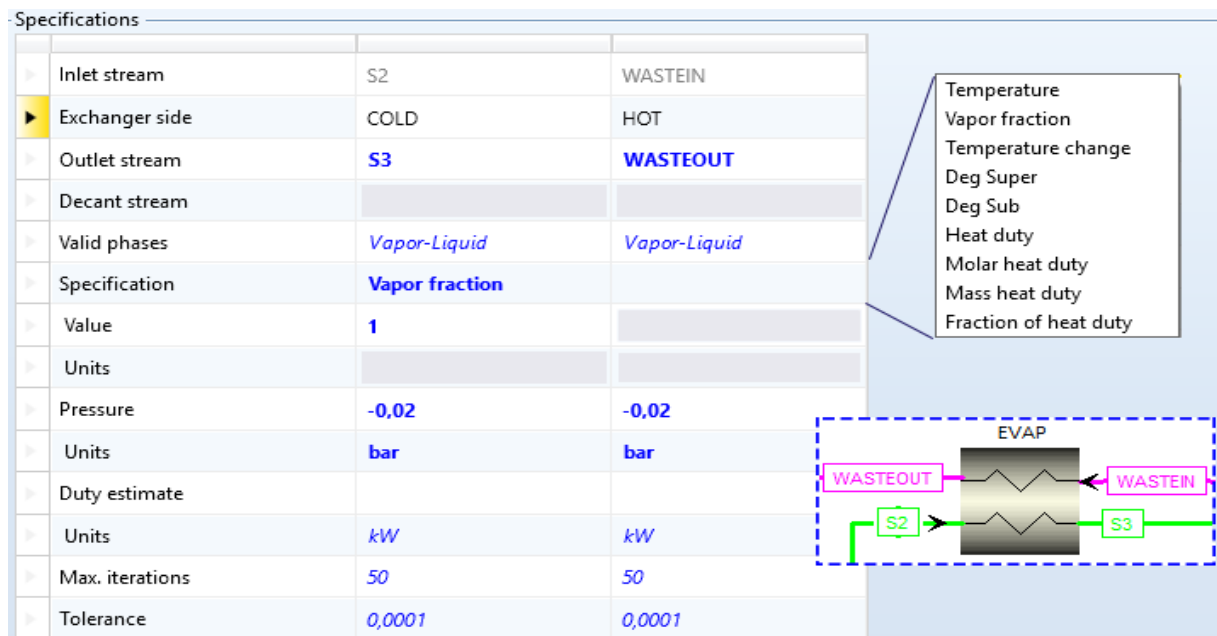


Fig. 30: Available settings for a multi-stream heat exchanger.

As a matter of facts, the two kind of exchangers have been setup to perform evenly and their choice depended only on aesthetic aspects.

3.3.3. Parameters' setup

Here, set values for the main thermodynamic parameters are listed. Also, the paragraph shows the user-defined scripts both in Calculator Blocks and Design Specs (their role has been introduced in [Par. 3.2](#)).

The cleaning section consists of a blower, 2 chillers (to dehumidificate up to dew point), 4 metal reactors in lead-and-lag configuration for the Sulphur-siloxanes removal, 2 scavengers in lead-and-lag configuration for ultra-filtration, 1 oil-free compressor.

This section is designed to accomplish the requirements on biogas quality: the fuel cell manufacturer requested as many pollutants as

- Sulphur < 30 ppb

- Siloxanes < 10 ppb

As previously stated, the aim of this work is focused on the energetic analysis of the system. Thus, only the power consumption of biogas blowing/compression was taken into account while the filtration was simply considered as a pressure drop and no pollutant were specified in the molar composition since the final values are within requirements.

Power consumption for this task has been calculated equal to 3.5 kW c.ca, while a total pressure drop of 200 mbar has been considered. Molar composition of the downstream biogas is showed in Tab. 5, Par. 3.3.2.

The operating principle of the system and the fuel path have been already described. Here below a summary table with the main parameters setup for each component (remember that positive pressure counts as the output state while negative ones as pressure drop).

	Pressure [mbar]	2 nd Parameter	
Blower	150 (increase)	$\eta_{is}=0,9$ $\eta_{mec}=0,95$	SOFC
Chiller	-50	25°C (T _{out})	
S-Removal	-50	-	
Scavengers	-50	-	
Fuel Compressor	4.1x10 ³ (discharge)	$\eta_{is}=0,9$ $\eta_{mec}=0,95$	
Dew-Chiller	-50	5°C (T _{out})	
Ejector	1.14 x10 ³ (discharge)	-	
Ext. Reformer	-20	650°C	
Fuel pre-Heater	-10	20°C (Pinch point)	
Int. Reformer	-20	850°C	
Anode	-20	850°C	
Air Compressor	1.12 x10 ³ (discharge)	$\eta_{is}=0,9$ $\eta_{mec}=0,95$	
Air pre-Heater	-10	218°C (Hot Stream out)	
Cathode	-20	100% O ₂ on 1 output	
After Burner	-30	Adiabatic Combustion	
Pump	Variable pressure	$\eta_{mec}=0,7$ $\eta_M=0,98$	ORC
HRU	-20 (both sides)	x=1 (output vapour frac.)	
Turbine	Condens. Pres. (discharge)	$\eta_{is}=0,85$ $\eta_{mec}=0,98$	
Condenser	-50	x=0 (output vapour frac.)	

Tab. 6: Main parameters summary for simulation components.

I remind here that most of design values were unknown so they have been hypothesized - based on literature and commercial standards – as starting values. The usefulness of Calculator blocks in Aspen Plus® is also that defined parameter can be exported and overwritten on previously initialized input data.

CONVION declared that $60 \text{ Nm}^3/h$ of biogas were the fuel needing for the 3 cells system. By supposing (at rated power):

- operating voltage of 0.7 V
- current density of 0.4 A/cm^2
- fuel utilisation factor of 80%

from equations (22) and (23) we have an Area of about $20.5 \text{ m}^2/\text{module}$, a total fuel flow of $55 \text{ Nm}^3/h$ and a stoichiometric oxygen flow of $0.22 \text{ mol}_{\text{O}_2}/\text{s}$ per module.

Variable name	Info. flow	Definition
IMODULE	Export	Parameter Parameter no.=1
CDENS	Export	Parameter Parameter no.=2
ASR	Export	Parameter Parameter no.=3
NFUEL	Export	Mole-Flow Stream=F-IN Substream=MIXED Component=CH4 Units=kmol/sec
NO2	Export	Stream-Var Stream=SOFC-3.O2 Substream=MIXED Variable=MOLE-FLOW Units=kmol/sec
FUELPARA	Export	Parameter Parameter no.=10

Define
Calculate
Sequence
Tears
Stream Flash
Information

Calculation method
 Fortran Excel

Enter executable Fortran statements


```

FARAD=96485333
FU=0.8
Atot=20.7e4

CDENS=NFUEL*8*FARAD*FU/(3*Atot)
IMODULE=CDENS*Atot

C
NFUEL=3*IMODULE/(8*FARAD*FU)
NO2=IMODULE/(4*FARAD)
FUELPARA=NFUEL
          
```

Fig. 31: C-MAIN block definition.

Starting from Oxygen stoichiometric value, it is possible to assess the required airflow. Actually, the air does not provide oxygen for the chemical reduction

only, but also removes the excess heat from the core in order to keep constant the reactor temperature. This means that as much air as it can bear the excess thermal power in limited temperature difference has to be blown into the system. In other words:

$$\dot{Q}_{waste} = \dot{m}_{air} c_{p,air} \Delta T_{air} = \dot{Q}_{air} \quad (35)$$

Here $c_{p,air}$ is a physical property, while ΔT_{air} is supposed to be $120^{\circ}C$ (see Tab. 3). Still, to find the fitting air mass flow we need to know how much is the produced thermal power. And this depends on the gases flow that enter the reactor.

At the same time, the mixture feeding the fuel cell must be stable in terms of carbon deposition at solid phase and prevent pore blocking. Usually a steam to carbon ratio (SC) around 2 is adopted, by means of a designed recirculation branch of steam-rich exhausts.

These two conditions are interdependent and iteratively solved by the code through ad hoc "Design Specs". The target conditions can be summarized - with relevant terms to the code - by the following equations:

$$\dot{Q}_{waste} = |\dot{Q}_{SOFC}| - |W_{SOFC}| - |\dot{Q}_{INT-REF}| = \dot{Q}_{air} \quad (36)$$

$$SC = \frac{\dot{n}_{H_2O}^{F10}}{\dot{n}_{CH_4}^{F10}} = 2 \quad (37)$$

where \dot{Q}_{SOFC} is the total enthalpy in the SOFC, W_{SOFC} is the fraction converted into electrical energy, $\dot{Q}_{INT-REF}$ is the heat required by internal reforming, $F10$ is the flow entering the external reformer (see also Fig. 22) .

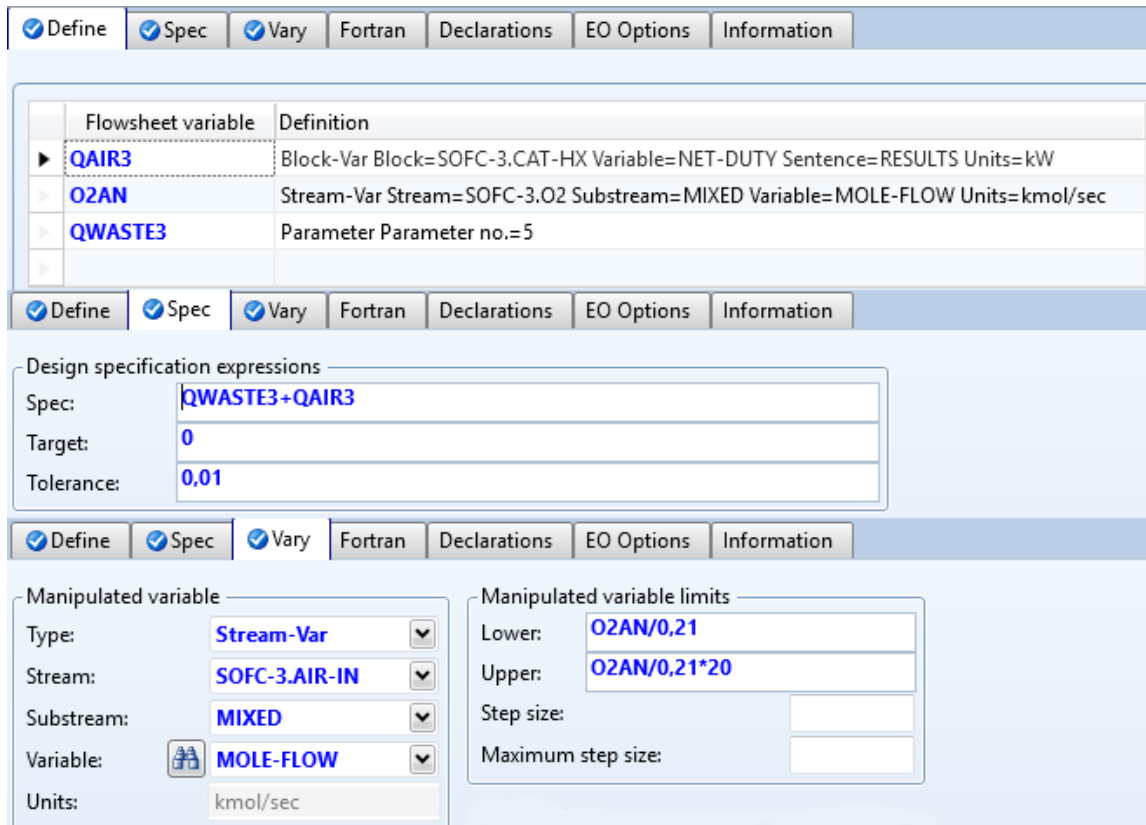


Fig. 32: Design Spec to research air mass flow value.

Nowadays most applications have an air utilization factor AU around 20% (5 times stoichiometric value). As you can see in Fig. 32 above the calculation was performed in a range up to 20 times to get to the result for sure.

The computation ended as follows:

$$AU = \frac{\dot{n}_{air}^{stoich}}{\dot{n}_{air}^{feed}} = \frac{\frac{\dot{n}_{O_2}^{stoich}}{y_{O_2}}}{\dot{n}_{air}^{feed}} \cong \frac{2.15 \cdot 10^{-4} kmol/s}{72.5 \cdot 10^{-4} kmol/s} \cong 14.1\% \quad (38)$$

Fraction of recirculated exhausts: 56% *c. ca.*

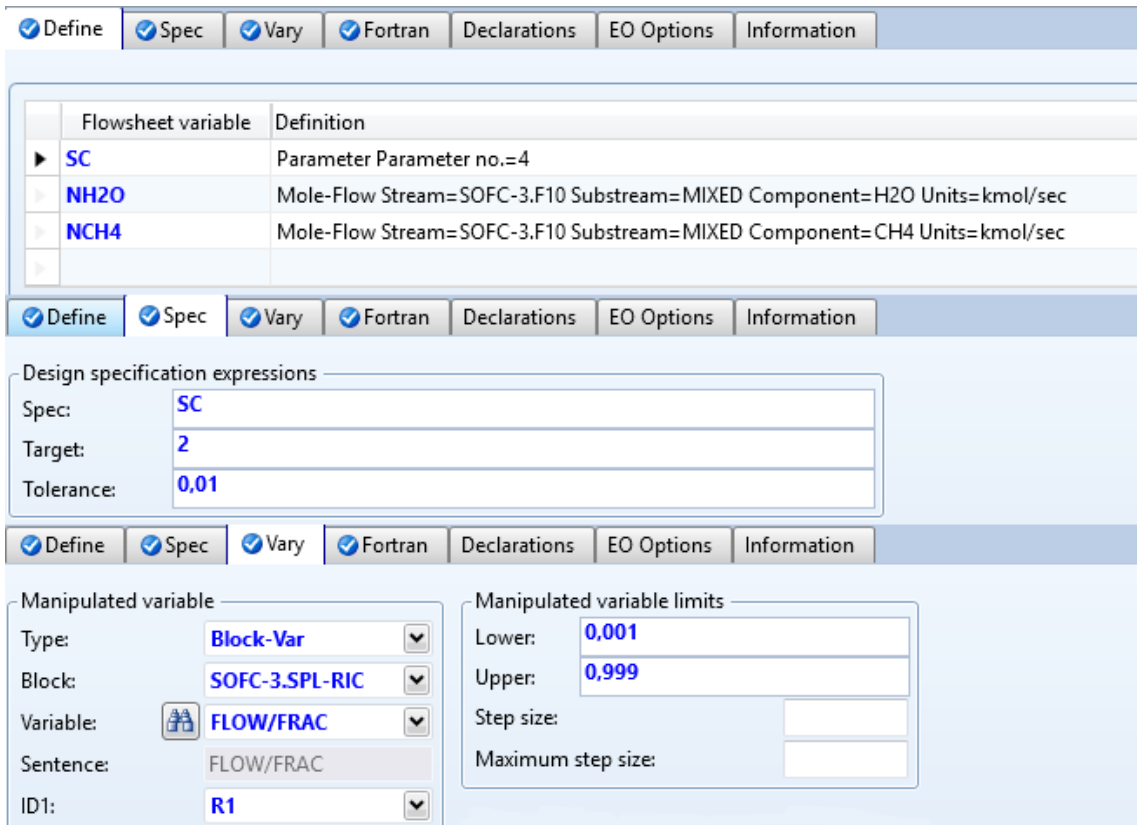


Fig. 33: Design Spec to assess recirculation fraction.

Power production and efficiency of the fuel cell were calculated in the calculator block “C-POWER”. It gathers the application of equation set from (6) to (26), properly translated into Fortran programming language, so it would not be of further interest to report the whole script. Nevertheless, it could be curious to know that the Fortran solver in Aspen Plus® (V8.0) shows some limit. For example, it doesn’t support nested arguments above a certain level or complexity. Nor it supports the “asinh” function, even if it exists as a Fortran function. Because of these reasons, some arguments have been splitted into simpler ones, while “asinh” function that appears in Eqq. (11) and (12) has been substituted with its approximation:

$$\operatorname{asinh}(x) \cong \log \left(x + \sqrt{x^2 + 1} \right) \quad (39)$$

Referring to the ORC flowsheet (Fig. 29), temperature and liquid status have been specified for stream S1. In this way pressure value is automatically computed through Aspen Plus® internal catalogue, being the pressure unique

with temperature on the saturation curve. Indicated mass flow is a first attempt value.

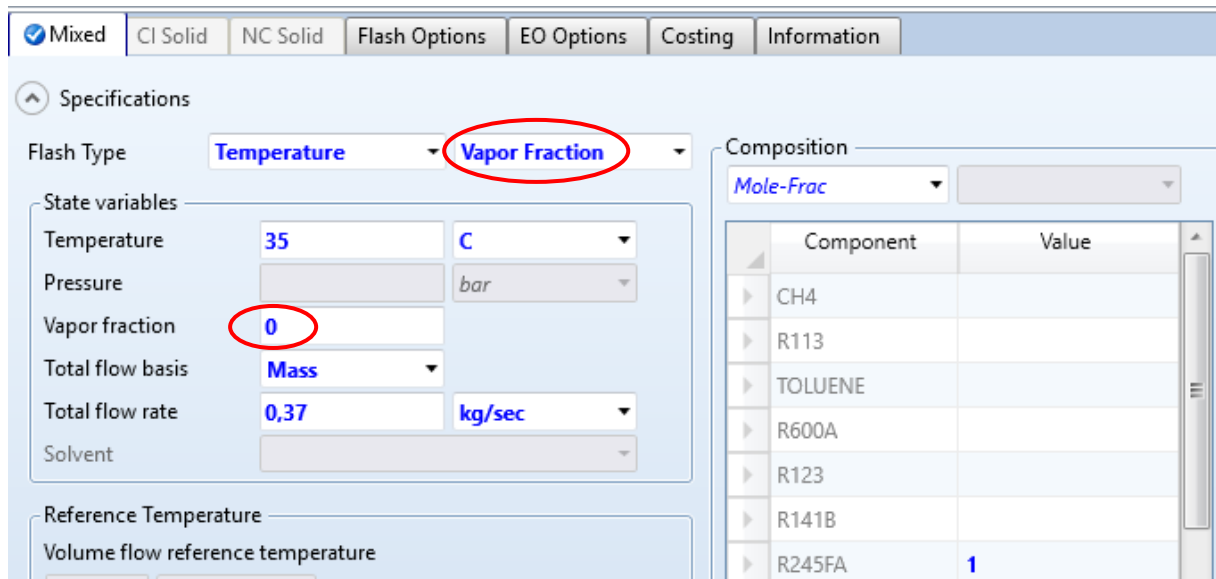


Fig. 34: S1 stream parameters for ORC subsystem.

Initially, the cycle was configured with a peak pressure just below the critical one for each working fluid (e.g. 36.3 bar for R245fa).

The EVAP only relevant parameter to be set was the status of the organic liquid at its output, i.e. saturated vapour, as shown in Fig. 30.

Finally, the expansion exploits all available enthalpy since no recovering of de-superheating energy was designed. This was done through a calculator block – called “ORC-LOOP” - which adapts the lowest pressure to that of the condensation (plus pressure drops within the condenser).

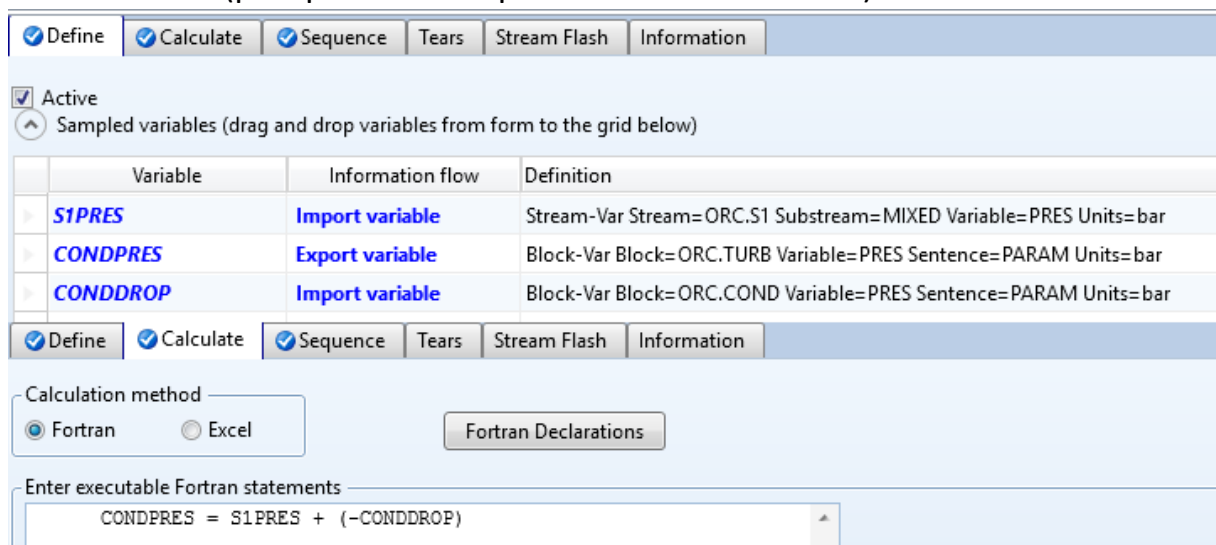


Fig. 35: ORC-LOOP Calculator Block for parameters continuity.

4. Results

In this chapter the results of the simulation and their argumentation is presented.

First step consisted of the validation of the SOFC model and the chosen parameters: it must satisfy theoretical model and place near CONVION nominal outputs at the same time. The latter thanks to the fact that as much complex or unknown the internal configuration could be, the working principle still follow the same laws.

Thus, with a feeding flow of $55 \text{ m}^3/\text{h}$ of biogas, an active area of 20.7 m^2 , 80% of fuel utilisation and a steam to carbon ratio set equal to two (2) I obtained:

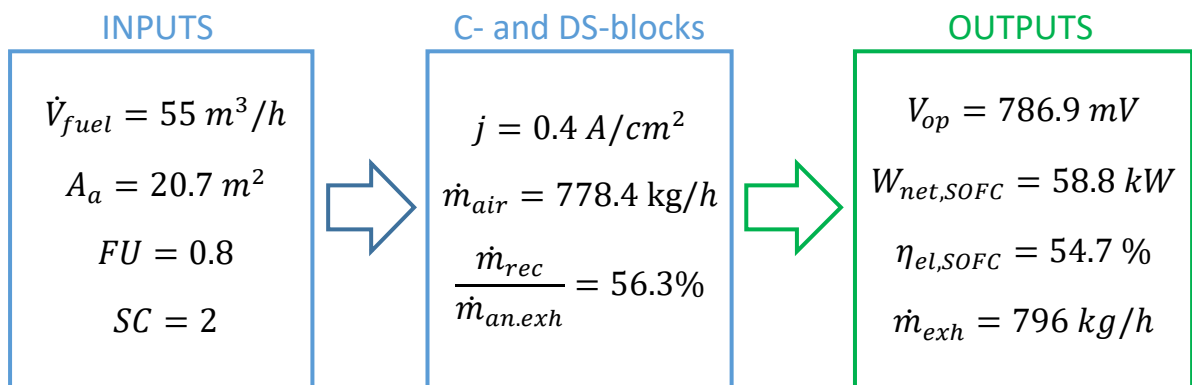


Fig. 36: SOFC model validation for nominal working point

These results are quite similar to those declared by CONVION, except for the needed air flow, thus the exhaust flow.

In particular:

- 58.7 kW VS 58 kW of produced power.
- 54.6 % VS 53% for net electrical efficiency (DC-AC inverter and air compressor included).
- 778 kg/h VS 601 kg/h for air mass flow. This is strictly related to the heat produced within the cell and the physical configuration of the internal heat exchangers. In fact, despite of the number of components from a functional point of view, commercial fuel cells are relatively compact systems. The internal geometry and the path of the gases can be such that a relevant fraction of the heat is recovered to feed the endothermic steam reforming

and to preheat both incoming fuel and air (e.g. in Fig. 37). That said, it would be really difficult to emulate internal heat distribution without design information.

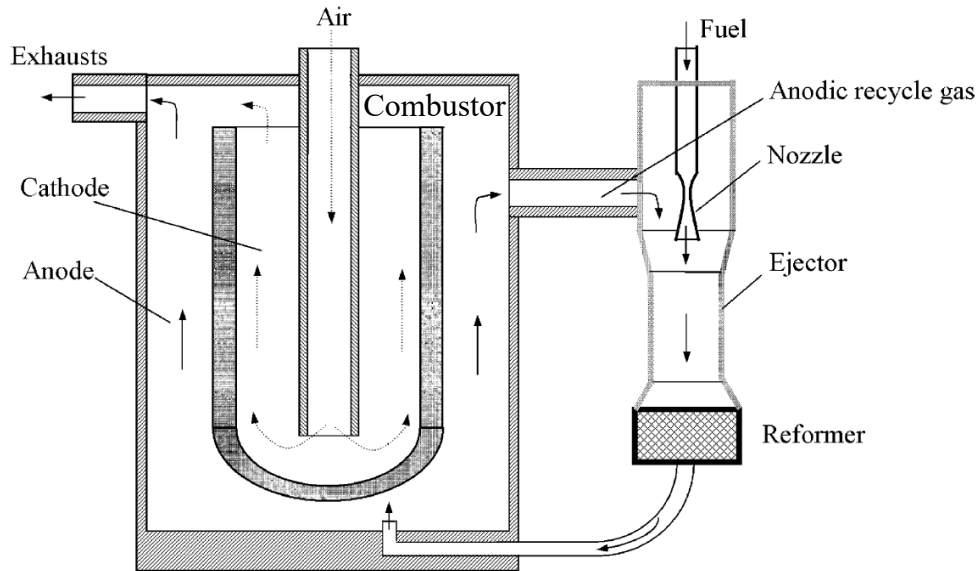


Fig. 37: Simplified sketch of a tubular SOFC module with anodic recirculation by an ejector.

The simulation investigated also different values of FU and temperature. In the first case, with lower fuel utilization and equal fuel feeding (this is a known starting point!) the cell works at lower current density. Therefore, the operating voltage is a bit higher, but the overall produced power and oxidation heat are lower. Nevertheless, methane and hydrogen content in the exhausts is higher, and much more heat is generated in the after burner. As you can see in picture above (even if referring to tubular configuration, the concept is valid for planar cells too) combustor is usually adjacent to the core so the produced heat has been taken into account for the energy core balance. As a result, the overall heat to be removed is higher compared to the case with higher FU and so the air flow. On the contrary, it would not be realistic to explore FU values higher than 80%. When exploring different values of temperature instead, power outputs are the ones moving away from nominal outputs.

A further investigation to get to results as closest as possible to CONVION system would have got too long and useless to the purpose, which remains the analysis of a SOFC-ORC hybrid system and the assessment of its overall benefits in terms of electrical power production compared to the base case.

This study is independent from the DEMOSOFC case since it provides results that fall within a range conceivable for any real case. That is why staying perfectly

close to the actual performances of the installed system is not relevant beyond a certain point, while some real input parameters can be still a good reference to start with.

With these premises, I chose to keep input parameters summarized in Fig. 36 and proceed with a sensitivity analysis based on current density variation in order to validate the electro-chemical model.

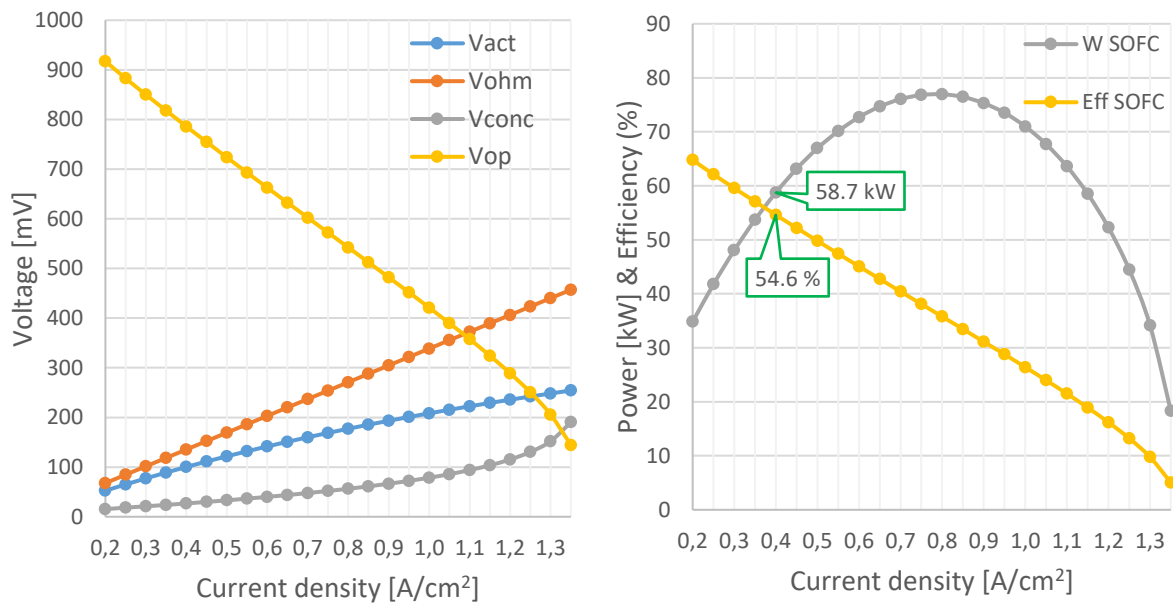


Fig. 38: SOFC model sensitivity analysis based on Current Density variation (constants: $FU=0.7$, $T=850^{\circ}C$).

Left graph of Fig. 38 shows the operative voltage curve with current density and the single loss contributions: ohmic loss is linearly proportional, and preponderant in the “central” range; activation losses have more influence on low values, as you can expect because of the ‘asinh’ function into its definition (11) and (12); on the other hand concentration losses are heavier for high current densities because of the logarithmic term (16) and (17). Usually they are neglected since fuel cells do not operate with currents too high. In addition, concentration effect is likely included in the Nernst equation (7) since at higher currents partial pressure of products tends to overcome on reactants one.

Right graph features power and SOFC efficiency: at constant FU and pressure fuel flow arises with current density (23) and more charges are reduced at the cathode. This implies a gain of current while voltage decreases with growing losses and power trend is explained. Efficiency monotonically decreases as well as losses monotonically increase.

When delivered current reaches a certain value ions migration through the electrolyte cannot withstand the kinetic of semi-reactions, so no more power is

produced. That is why it is called limiting current, and it physically provokes the device to switch off. Anode limiting current is proportional with hydrogen partial pressure at the bulk and diffusivity – and inversely with temperature, but here it is constant - so slightly increasing with fuel flow. In this case it stops around 1.39 A/cm^2 , consequently the simulation was stopped at 1.35 A/cm^2 .

Consistently with what it has been done above, validation of ORC model is shown hereunder. For compactness purposes, demonstration graphs are presented for one fluid only (R245fa).

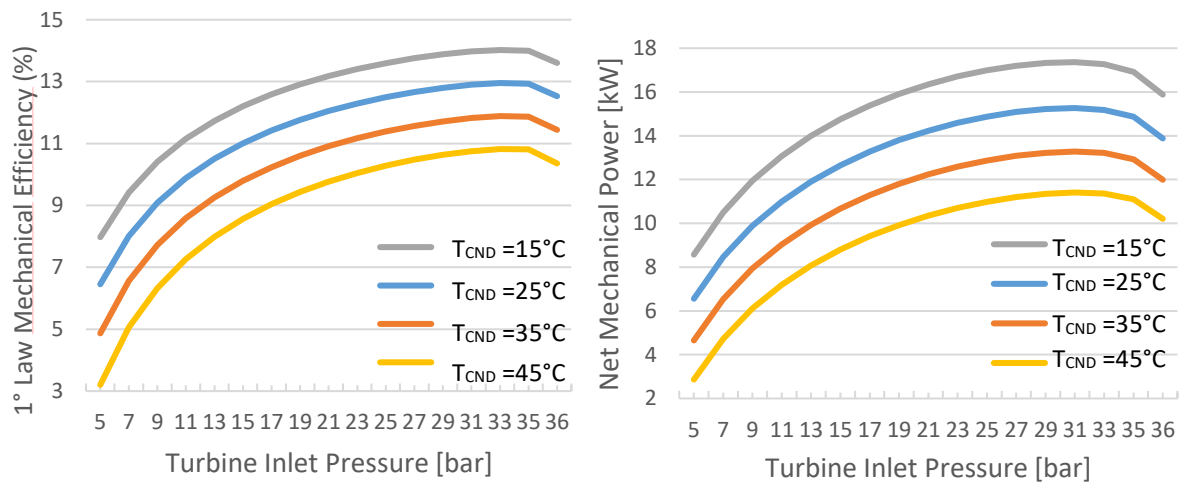


Fig. 39: ORC model validation: Mechanical efficiency and power VS Turbine inlet pressure.

Enthalpy availability for expansion work rises along with turbine inlet pressure and lower condensing temperature, so the produced power and efficiency. When the peak pressure approaches critical value, gained heat does not grow enough to compensate higher pump needing, so the efficiency reverses its trend.

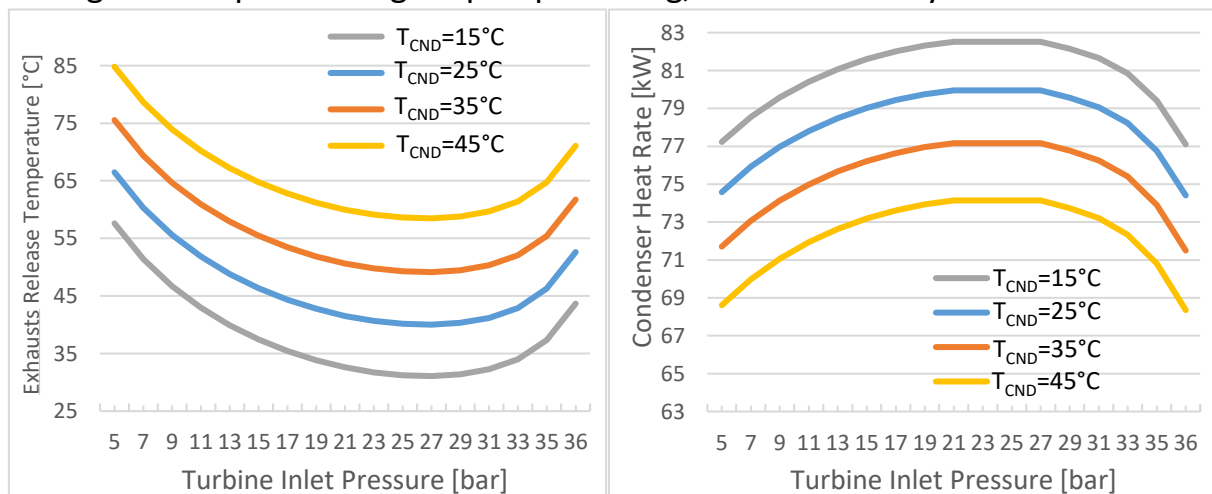


Fig. 40: ORC model validation: SOFC final waste temperature and Condenser heat rate VS Turbine inlet pressure.

Condenser heat is more substantial with lower temperature due to wider base of the saturation curve (latent heat). On the opposite, recoverable heat grows with colder fluid at the pump, thus exhaust gases are as colder as lower is the ORC condensing temperature.

SOFC modules exhausts feed ORC sub-system without any further energy request, thus the bottom cycle can influence whole system efficiency only by means of power production. Based on this criterion, performances have been investigated by varying evaporator pressure and fluid mass flow. Also, influence of the latter on exchanging area size – see also costs - has been taken into account by introducing a constraint on minimal temperature approach at the evaporator greater or equal to 10°C. Minimal temperature approach on condenser side was intrinsically considered through the setup of the lowest temperature, given the considerations about ambient seasonal variation (see page 43).

Hereunder common optimization process and the results for each selected organic fluid is illustrated (you will read mean values, significant for all four seasons).

The screenshot displays the Aspen Plus optimization interface, divided into three main sections:

- CONSTRAINT DEFINITION AND SPEC:** Shows the definition of the variable **EVAPMITA** as `Block-Var Block=ORC.EVAP Variable=MITA Sentence=RESULTS Units=C`. A constraint is defined with the specification **Greater than or equal to** and a value of **10**, with a tolerance of **0,1**.
- OPTIMIZATION OBJECTIVE AND VARY:** Shows that optimization is active and set to **Maximize** the objective function **ORCWNET**. The constraint **C-PINCH** is selected for optimization.
- Table of Manipulated Variables:** A table listing the variables to be varied during optimization.

Variable	Active	Manipulated variable	Lower limit	Upper limit	Units
1	<input checked="" type="checkbox"/>	Block-Var Block=ORC.PUMP Variable=PRES Sentence=PARAM	0.15*PCRIT	0.95*PCRIT	bar
2	<input checked="" type="checkbox"/>	Mass-Flow Stream=ORC.S1 Substream=MIXED Component=R245FA	0.1	1	kg/sec

Fig. 41: Aspen Plus® optimization process to maximize power production.

- R141b (1,1-dichloro-1-fluoroethane, isentropic)
Pump discharge pressure: 28.5 bar
Fluid mass flow: 0.35 kg/s
ORC MAX supplemented power: 21.0 kW @ $T_{CND} = 15^{\circ}C$
Minimal condensing pressure: 0.54 bar @ $T_{CND} = 15^{\circ}C$
- R245fa (1,1,1,3,3-pentafluoropropane, isentropic)
Pump discharge pressure: 31.6 bar
Fluid mass flow: 0.42 kg/s
ORC MAX supplemented power: 16.6 kW @ $T_{CND} = 15^{\circ}C$
Minimal condensing pressure: 1.01 bar @ $T_{CND} = 15^{\circ}C$
- R123 (2,2-dichloro-1,1,1-trifluoroethane, isentropic)
Pump discharge pressure: 30.2 bar
Fluid mass flow: 0.46 kg/s
ORC MAX supplemented power: 19.3 kW @ $T_{CND} = 15^{\circ}C$
Minimal condensing pressure: 0.62 bar @ $T_{CND} = 15^{\circ}C$
- R600a (Isobutane, dry)
Pump discharge pressure: 31.3 bar
Fluid mass flow: 0.25 kg/s
ORC MAX supplemented power: 14.4 kW @ $T_{CND} = 15^{\circ}C$
Minimal condensing pressure: 2.57 bar @ $T_{CND} = 15^{\circ}C$
- Toluene (Isentropic), flammable
Pump discharge pressure: 34.2 bar
Fluid mass flow: 0.15 kg/s
ORC MAX supplemented power: 24.4 kW @ $T_{CND} = 15^{\circ}C$
Minimal condensing pressure: 0.02 bar @ $T_{CND} = 15^{\circ}C$
- R113 (1,1,2-Trichlorotrifluoroethane, Isentropic), flammable
Pump discharge pressure: 30.3 bar
Fluid mass flow: 0.45 kg/s
ORC MAX supplemented power: 20.5 kW @ $T_{CND} = 15^{\circ}C$
Minimal condensing pressure: 0.31 bar @ $T_{CND} = 15^{\circ}C$

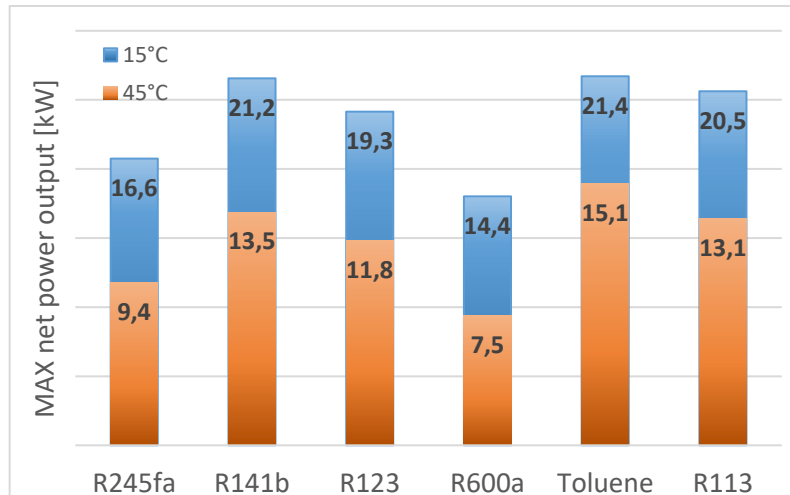


Fig. 42: Minimum ($T_{CND} = 45^{\circ}C$) and maximum ($T_{CND} = 15^{\circ}C$) electrical power output comparison.

Provided that the objective function to maximize here is the rated power, the maximum working pressure, the total heat transfer area and the expander size are three important technical and economic factors in ORC system and they were considered in the analysis.

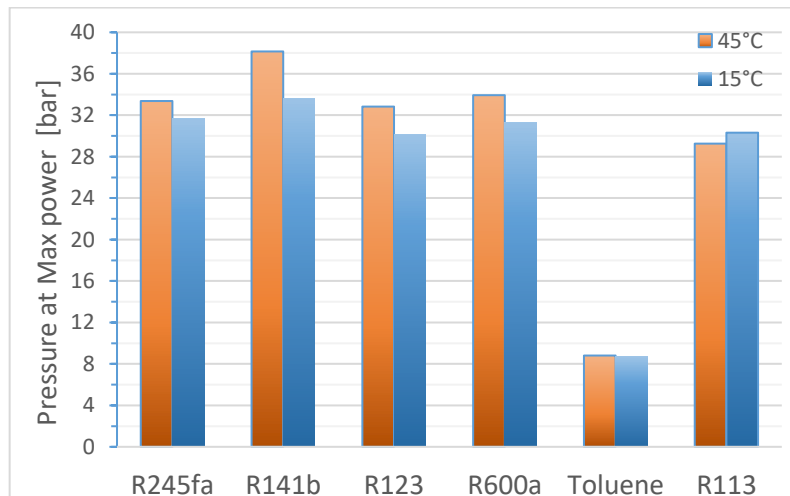


Fig. 43: Turbine inlet (evaporation) pressure range at the maximal power output.

The reader could deduct from Fig. 42 and Fig. 43 that the most suitable fluid is Toluene, given the highest power rating and the lowest evaporation pressure. Nevertheless, it is necessary to check also condensation pressure since many organic fluids have very low saturation pressures at ordinary environment temperature.

In fact, in this case not only Toluene, but also R113 condensates far below atmospheric pressure in any season. As regards R141b and R123 depression is verified for $T_{CND} = 15^{\circ}C$ and $T_{CND} = 25^{\circ}C$, while it is not above $30^{\circ}C$ (Fig. 44).

This is a relevant aspect to take account of, given that a perfect sealed system leads to higher cost as much as lower is the operating pressure.

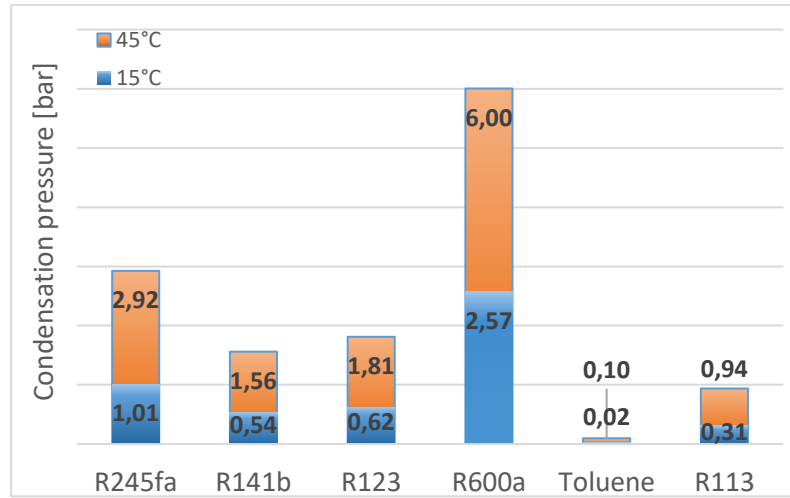


Fig. 44: Condensation pressure range at extremity imposed conditions.

The total heat transfer capacity $(UA)_{tot}$, which has been used to evaluate the cost of heat exchangers, can approximately reflect the total heat transfer area of heat exchangers in the ORC system [36], [37]. The $(UA)_{tot}$ could be evaluated by the following equations:

$$(UA)_{tot} = \frac{\dot{Q}_{evp}}{\Delta T_{me}} + \frac{\dot{Q}_{cnd}}{\Delta T_{mc}} \quad (40)$$

$$\dot{Q}_{evp} = \dot{m}_{wf} |\Delta h_{evp}| \quad (41)$$

$$\dot{Q}_{cnd} = \dot{m}_{wf} |\Delta h_{cnd}| \quad (42)$$

$$\Delta T_m = \frac{\Delta T_{MAX} - \Delta T_{min}}{\ln \left(\frac{\Delta T_{MAX}}{\Delta T_{min}} \right)} \quad (43)$$

where \dot{Q}_{evp} and \dot{Q}_{cnd} are the heat rate injected and rejected, respectively, ΔT_m is the logarithmic mean temperature difference, ΔT_{MAX} and ΔT_{min} are the maximal and minimal temperature differences at the ends of the heat exchangers, respectively. Macchi [38] used the expander SP to evaluate the expander size.

$$SP = \frac{\sqrt{\dot{V}_{S4s}}}{\sqrt[4]{\Delta H_s}} \quad (44)$$

where \dot{V}_{S4S} is the volume flow rate of the working fluid at the end of the corresponding isentropic expansion (see stream 'S4' in Fig. 29) and ΔH_s is the specific isentropic enthalpy drop in the expander.

The Size Parameter is relevant in turbine design together with the volume ratio of the stages. In particular, at a fixed value of volume ratio, the isentropic efficiency of a turbine grows with the SP. On the other hand, mean radius grows as well, so the dimensions, so the cost. That is why a good compromise must be chosen.

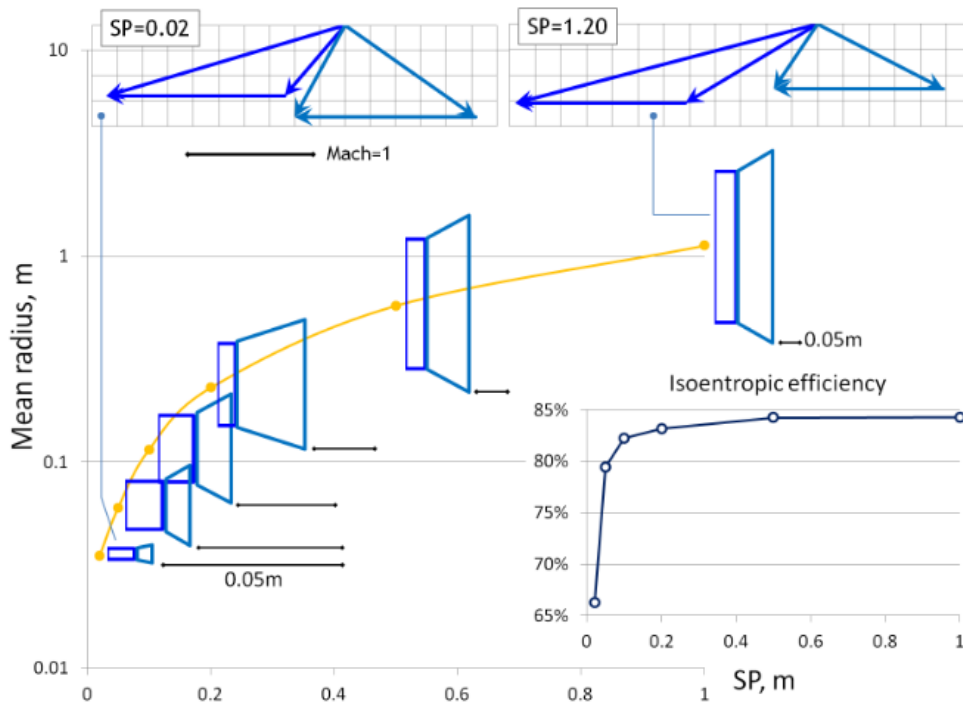


Fig. 45: Correlation between Size Parameter and turbine efficiency/dimension [39].

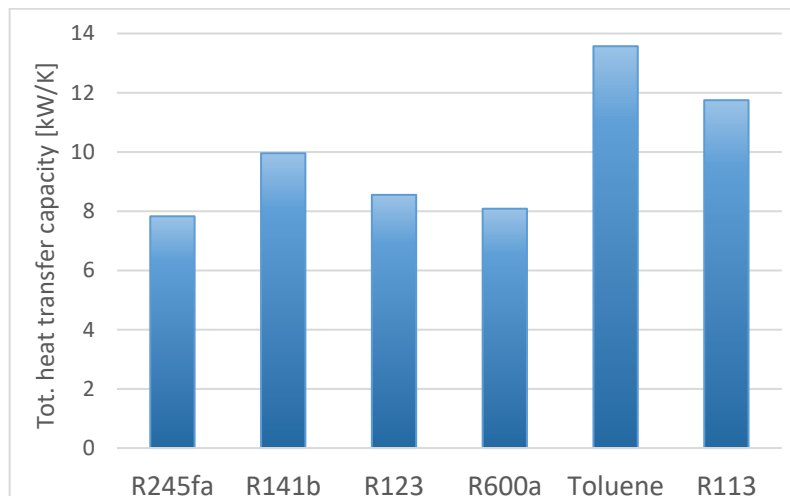


Fig. 46: Simulated Total Heat Transfer Capacity with selected working fluids.

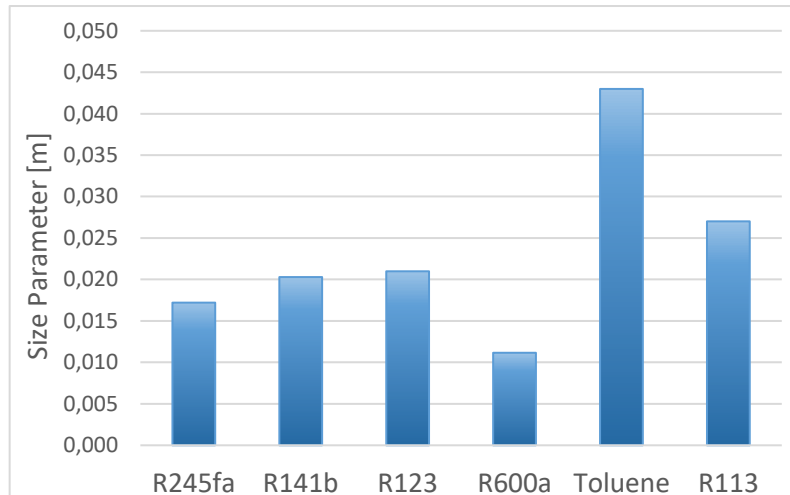


Fig. 47: Simulated expander Size Parameter with selected working fluids.

Fig. 46 and Fig. 47 illustrate the total heat transfer capacity and the expander SP of the optimization routine – i.e. at maximum power.

Toluene reaches the highest value, up to 13.6 kW/K for lowest ambient temperature, because of its lowest mean logarithmic temperature difference at the evaporator, where the biggest heat rate is exchanged. R113 shows similar results, even if the heat capacity is slightly below 12 kW/K . These two fluids have the highest critical temperatures among the selected ones. Toluene's T_{Cr} is far above the temperature of the waste heat source, while that of R113 is few degrees below it. Thus their saturation temperature at the turbine inlet is really close to the one of the SOFC exhausts, keeping the mean temperature difference at the minimum (40). For R141b the range stands around 10 kW/K while R123 and Isobutane are just above 8 kW/K . R245fa has the lowest value, with benefits from an economic point of view.

As shown in Fig. 47, for Isobutane the expander SP is not greater than 0.01 m . For working fluids R245fa, R141b and R123, the range of the expander SP is from 0.01 m to 0.02 m . The Size Parameter is greater than 0.025 m for toluene and R113. In fact, because of the really low condensation pressure, the specific volume is much higher for the two latter fluids compared to the other ones, and so the volume flow which is the numerator in the SP definition (44).

To recap, ORC based Toluene and R113 has a minimal pressure much lower of the atmospheric one with any of the imposed condensation temperatures (Fig. 44). This would require a perfect sealing to avoid leakage, so a higher cost for the plant. In R600a case, the lowest power gain is registered, as well as the

lowest expander SP (Fig. 47), which probably means a lower isentropic efficiency (to state that, a double check on the volume ratio should be done too).

Among the remaining three, R245fa is the only one that presents not depression cases and requires less expensive exchangers (Fig. 46), while R141b provides the highest power (Fig. 42). Nevertheless, even imposing a condensation pressure as high as the atmospheric one, the simulation with R141b still gives back a computed power equal to 16.3 kW , that is only 0.3 kW below the best result ($T_{CND} = 15^\circ\text{C}$) of R245fa case.

Based on the above discussion, it could be concluded the R141b is the best candidate under given conditions, even if limiting the operating range by imposing a minimal condensation pressure of 1 atm . The ORC system in fact could still produce from 13.5 kW to 16.3 kW , which is the best result once Toluene and R113 are excluded. Since the reference case has a computed power output of 172.8 kW , this would mean a relative efficiency increment of 7.82% to 9.45% .

5. Conclusions

A process model of a hybrid system via Aspen Plus® code is proposed to evaluate performance improvements of a Solid Oxide Fuel Cell reactor. The reference conditions are based on a real project – DEMOSOFC - installed in a WWTP in Turin, northern Italy. A biogas flow is available downstream of a bio-digesting and cleaning process, and feeds three SOFC modules, which consume around $60Nm^3/h$ of fuel as a whole.

Computed results give a rated power of $58.8 kW$ per module and about $3.6 kW$ consumed by the auxiliaries of the cleaning section, which make $172.8 kW$ for the DEMOSOFC system. About $3,300 Nm^3/h$ of flue gases flow out, mainly consisting of hot air and some water plus unreacted fuel. Their temperature is $220^\circ C$, thus a sub-critic ORC is identified for waste heat recovery and net power maximization.

Performances of six working fluids are investigated, as well as the optimization is implemented in the code and the Complex algorithm is used. The maximum net power output, suitable working pressure, total heat transfer capacity and expander SP are considered as the criteria to screen the working fluids.

The main conclusions are made as follows:

- The maximum net power output varies at the given conditions, from $7.5 kW$ in the hot season to $21.4 kW$ in winter, when R600a and Toluene are used, respectively. R141b, R113 and R123 give high rates too, while R245fa performs a bit better than Isobutane. It is generally observed what theory suggests: fluids whose critical temperature approaches that of the waste heat source provide greater power. Toluene is an exception, since it has a critical temperatures that far surpasses $220^\circ C$, but it has a drawback that is explained hereunder.
- ORC presents a range of evaporation pressure going from $29.5 bar$ to $34 bar$ for R113, R123, R600a and R245fa. Among these, Isobutane cycle records the highest P_{evp}/P_{cr} ratio, up to 97.5%, being the one with the lowest T_{cr} . The peak is observed at $38.1 bar$ and is reached with R141b, which has the greatest critical pressure. On the contrary, inlet turbine pressure stops at $8.8 bar$ when Toluene is used, because of its saturation curve: the isobars are

gathered towards the top of the bell, so the saturation temperature is high enough at pressure as low as 8 *bar*.

- Cycles of R245fa and R600a are the only ones with condensation pressures equal or above the atmospheric one in any case. R141b and R123 operate down to 0.54 *bar* when condensation temperature is set up to 15°C and 25°C. Toluene and R113 instead, show always the minimal pressure much lower than that of the external environment, especially Toluene to an order of 10^{-2} *atm*. In order to inspect an alternative way to pipework sealing – read costs - a further simulation with a lower bound on the pressure has been run for these two fluids, but the new computed net power wiped out their attractiveness, hence they were excluded.
- Total heat transfer capacity is higher for Toluene and R113 (13.6 *kW/K* and 12 *kW/K*, respectively), because of their high critical temperature, which keeps the mean logarithmic difference at the minimum at the evaporator side. As expected from a sub-critical ORC, the opposite is true as well, in fact R245fa presents the lowest value (7.8 *kW/K*). R141b is coherent with its critical temperature, which makes it attest below R113. Even if R600a has the lowest critical temperature, condensation latent heat is much higher and so the rejected heat rate. This brings its capacity as high as the one of R123, around 8.7 *kW/K*.
- All computed values for expander SP fall in a range below $45 \cdot 10^{-3}$ *m*, where the isentropic efficiency and the mean radius of the turbine can vary a lot. According to this parameter, R123 and R141b are better to be used, once Toluene and R113 are excluded.
- Based on the screening criteria above, R141b is the most suited working fluid in sub-critical ORC under the given conditions if a lower bound at atmospheric pressure is imposed. With such design, esteemed ORC net power and relative efficiency gain of the hybrid system on the base project range from 13.5 *kW* to 16.3 *kW* and from 7.82% to 9.45%, respectively.

Table of figures and tables

Fig. 1: From International Energy Agency (IEA) website.	4
Fig. 2: Renewables share of power generation, from BP Energy Outlook (2016).	5
Fig. 3: FP7 funding for different NNE sectors.	6
Fig. 4: SOFC-GT-ST combined cycle, studied from Alexandros Arsalis [22].	8
Fig. 5: Generic layout of a system involving a SOFC integrated with an ORC cycle.	9
Fig. 6: T-s chart of n-Dodecane and Propane. Note the critical temperatures: next to 400°C and 100°C respectively.	10
Fig. 7: Layout of a SOFC–ORC system powered by syngas [24].	11
Fig. 8: A scheme of the combined SOFC-Stirling system fuelled by ammonia.....	13
Fig. 9: The effect of the SOFC fuel utilization factor (left) and operating temperature (right) on plant efficiency [25].	13
Fig. 10: Plant thermal efficiency and net power production as a function of woodchip mass: a) constant woodchip mass flow and b) constant SOFC electrical power [26].	14
Fig. 11: SOFC–AC–ORC–PTSC hybrid system layout [29].	16
Fig. 12: SOFC–ORC–AC hybrid layout [30].	18
Fig. 13: Schematic flow diagram of Collegno WWTP after DEMOSOFC realization.	20
Fig. 14: Pre-treatment section for biogas cleaning.	22
Fig. 15: CONVION C50 Solid Oxide Fuel Cell module.	23
Fig. 16: Schematic of C50 interfaces.	23
Fig. 17: Schematic diagram of studied SOFC-ORC system.	26
Fig. 18: Polarization curve of a fuel cell.	29
Fig. 19: SOFC unit-Grid interface.	31
Fig. 20: Component table defined in the Aspen code.	34
Fig. 21: Custom properties to be added in the streams results.	36
Fig. 22: Aspen Flowsheet for Convion C50 module.	37
Fig. 23: A mixer block and its settings.	38
Fig. 24: Settings of the Gibbs reactor as the external reformer.	39
Fig. 25: Settings for the air blower (single stadium compressor).	40
Fig. 26: Available settings for a two-stream heat exchanger block.	41
Fig. 27: Setting of the separator emulating the cathode. Oxygen only proceeds into stream O1 (O ²⁻ ions).	41
Fig. 28: Simple heat exchanger block. It helps in accounting for the right amount of cooling air.	42
Fig. 29: Flowsheet of the Organic Rankine Cycle section of the system.	43
Fig. 30: Available settings for a multi-stream heat exchanger.	44
Fig. 31: C-MAIN block definition.	46
Fig. 32: Design Spec to research air mass flow value.	48
Fig. 33: Design Spec to assess recirculation fraction.	49
Fig. 34: S1 stream parameters for ORC subsystem.	50

Fig. 35: ORC-LOOP Calculator Block for parameters continuity.....	50
Fig. 36: SOFC model validation for nominal working point.....	51
Fig. 37: Simplified sketch of a tubular SOFC module with anodic recirculation by an ejector.....	52
Fig. 38: SOFC model sensitivity analysis based on Current Density variation (constants: FU=0.7, T=850°C).....	53
Fig. 39: ORC model validation: Mechanical efficiency and power VS Turbine inlet pressure.	54
Fig. 40: ORC model validation: SOFC final waste temperature and Condenser heat rate VS Turbine inlet pressure.	54
Fig. 41: Aspen Plus® optimization process to maximize power production.	55
Fig. 42: Minimum ($T_{CND} = 45^{\circ}C$) and maximum ($T_{CND} = 15^{\circ}C$) electrical power output comparison.....	57
Fig. 43: Turbine inlet (evaporation) pressure range at the maximal power output.	57
Fig. 44: Condensation pressure range at extremity imposed conditions.	58
Fig. 45: Correlation between Size Parameter and turbine efficiency/dimension [39].	59
Fig. 46: Simulated Total Heat Transfer Capacity with selected working fluids.	59
Fig. 47: Simulated expander Size Parameter with selected working fluids.	60
Tab. 1: Biogas molar composition after digestion at Collegno SMAT plant.....	22
Tab. 2: Summary of typical C50 module outputs.	24
Tab. 3: SOFC input values that are fixed throughout the study.....	27
Tab. 4: Bossel constant parameters for common SOFC materials.....	30
Tab. 5: Comparison of the fuel composition downstream of the digester and upstream of the fuel cell.	38
Tab. 6: Main parameters summary for simulation components.	45

References

- [1] Eurostat, "Energy production and imports. [Online]," 2012. [Online]. Available: http://ec.europa.eu/eurostat/statistics-explained/index.php/Energy_production_and_imports.
- [2] EC, "The "20-20-20" targets. [Online]," 2010. [Online]. Available: http://ec.europa.eu/eurostat/statistics-explained/index.php/Europe_2020_indicators_-_climate_change_and_energy.
- [3] EC, "International cooperation with Mediterranean countries in FP7. [Online]," 2012. [Online]. Available: http://ec.europa.eu/research/conferences/2012/euro-mediterranean/pdf/international_cooperation_with_mpc.pdf.
- [4] J. L. S. J. H. K. T. S. K. S. T. R. K. S. T. W. Song, "Performance analysis of a tubular solid oxide fuel cell/micro gas turbine hybrid power system based on a quasi-two dimensional model," *Journal of Power Sources*, no. 142, pp. 30-42, 2005.
- [5] B. B. A. F. Massardo, "Assessment of molten carbonate fuel cell models and integration with gas and steam cycles," *Journal of Engineering for Gas Turbines and Power*, no. 124, pp. 103-109, 2002.
- [6] S. U. P. Lunghi, "Efficiency upgrading of an ambient pressure molten carbonate fuel cell plant through the introduction of an indirect heated gas turbine," *Journal of Engineering for Gas Turbines and Power*, no. 124, pp. 858-866, 2002.
- [7] T. S. K. K. S. Oh, "Performance analysis on various system layouts for the combination of an ambient pressure molten carbonate fuel cell and a gas turbine," *Journal of Power Sources*, no. 158, pp. 455-463, 2006.
- [8] S. C. P. Iora, "Development of a three-dimensional molten carbonate fuel cell model and application hybrid cycle simulations," *Journal of Fuel Cell Science and Technology*, no. 4, pp. 501-510, 2007.
- [9] M. D. L. S. T. J. H. Ghezal-Ayagh, "Dynamic modeling and simulation of a hybrid fuel cell/gas turbine power plant for control system development," *Fuel Cell Science, Engineering and Technology*, no. 2004, pp. 325-329, 2004.
- [10] H. A. A. Arnab Choudhury, "Application of solid oxide fuel cell technology for power generation - A review," *Renewable and Sustainable Energy Reviews*, vol. 20, p. 430-442, 2013.

- [11] F. A. Zabihian F, "A review on modeling of hybrid solid oxide fuel cell," *Int J Eng*, no. 3, pp. 85-119, 2009.
- [12] A. A. D. H. B. R. M. A. McPhail SJ, "SOFC and MCFC: commonalities and opportunities for integrated research," *Int J Hydrogen Energy*, vol. 36, 2011.
- [13] D. d. A. M. V. L. v. S. M. Calise F, "Full load synthesis/design optimization of a hybrid SOFC GT power plant," *Energy*, vol. 32, pp. 446-458, 2007.
- [14] C. S. L. G. H. H. L. J. F. Z. Zhang X, "A review of integration strategies for solid oxide fuel cells. J Power Sources 2010;195:685–702," *Journal of Power Sources*, vol. 195, pp. 685-702, 2010.
- [15] D. d. A. M. V. L. v. S. M. Calise F, "Single-level optimization of a hybrid SOFC GT power plant," *J Power Sources*, vol. 159, p. 1169–85, 2006.
- [16] S. C, *Design, operation and control modelling of SOFC/GT hybrid systems*, 2006.
- [17] R. M. E. B. Bang-Møller C, "Exergy analysis and optimization of a biomass gasification, solid oxide fuel cell and micro gas turbine hybrid system," *Energy*, vol. 36, p. 4740–52, 2011.
- [18] S. TP, *Hardware simulation of fuel cell/gas turbine hybrids*, 2007.
- [19] *220 kWe solid oxide fuel cell/microturbine generator hybrid proof of concept demonstration report*, Commission CE, March 2001.
- [20] S. L. D. J. G. J. L. W. Veyo SE, "Tubular solid oxide fuel cell/gas turbine hybrid cycle power systems: status," *J Eng Gas Turb Power*, vol. 124, p. 845–849, 2002.
- [21] Y. Q. J. T. Y. W. Zhao HB, "The performance analysis of combined cycle system driven by solid oxide fuel cell," *J Eng Thermophys*, vol. 35, p. 848–853, 2014.
- [22] V. S. M. C. F. Arsalis A, "Thermoeconomic modeling and parametric study of hybrid solid oxide fuel cell-gas turbine-steam turbine power plants ranging from 1.5 MWe to 10 MWe," *J Fuel Cell Sci Technology*, vol. 6, pp. 0110151-01101512, 2009.
- [23] B. S. Ali Volkan Akkaya, 16 December 2008. [Online]. Available: <http://onlinelibrary.wiley.com/doi/10.1002/er.1490/full>.
- [24] R. M. L. U. H. F. Pierobon L, "Thermodynamic analysis of an integrated gasification solid oxide fuel cell plant combined with an organic Rankine cycle," *Renew Energy*, vol. 60, pp. 226-234, 2013.
- [25] R. M, "Thermodynamic analysis of SOFC (solid oxide fuel cell) - Stirling hybrid plants using alternative fuels," *Energy*, vol. 61, pp. 87-97, 2013.

- [26] R. Masoud, "Biomass gasification integrated with a solid oxide fuel cell and Stirling engine," *Energy*, vol. 77, pp. 6-18, 2014.
- [27] M. Rokni, "Thermodynamic analyses of municipal solid waste gasification plant integrated with SOFC and Stirling hybrid system," *International Journal of Hydrogen Energy*, vol. 40, pp. 7855-7869, 2015.
- [28] P. Stouffs, "Does the Ericsson engine deserve more consideration than the Stirling engine?," in *Proceedings of the European Stirling Forum*, Osnabrück, Germany, 2002, p. 8.
- [29] D. I. Ozcan H, "Thermodynamic analysis of an integrated SOFC, solar ORC and absorption chiller for tri-generation applications," *Fuel Cells*, vol. 13, pp. 781-793, 2013.
- [30] D. I. H. F. Al-Sulaiman FA, "Thermoeconomic optimization of three trigeneration systems using organic Rankine cycles: part I – Formulations," *Energy Convers Manage*, vol. 69, p. 199–208, 2013.
- [31] D. I. H. F. Colpan Can Ozgur, "Thermodynamic modeling of direct internal reforming solidoxide fuel cells operating with syngas," *International Journal of Hydrogen Energy*, vol. 32, pp. 787-795, 2007.
- [32] B. UG, "Final report on SOFC data facts and figures," Swiss Federal Office of Energy, 1992.
- [33] V. A. F. K.-Z. M. K. S. S. Kim Jai-Woh, "Polarization effects in intermediate temperature, anode-supported solid oxide fuel cells," *Journal of the Electrochemical Society*, vol. 146, pp. 69-78, 1999.
- [34] L. C. D. O. Chan SH, "Energy and exergy analysis of simple solid-oxide fuel-cell power systems," *Journal of Power Sources*, vol. 103, pp. 188-200, 2002.
- [35] Wikipedia, «Equazione di stato,» [Online]. Available: https://it.wikipedia.org/wiki/Equazione_di_stato. [Consultato il giorno 22 01 2017].
- [36] W. H. Z. S. Guo T, "Comparative analysis of CO₂-based transcritical Rankine cycle and HFC245fa-based subcritical organic Rankine cycle using low-temperature geothermal source.," *Science China*, vol. 53, no. 6, pp. 1638-1646, 2010.
- [37] K. S. A. R. Schuster A, "Efficiency optimization potential in supercritical Organic Rankine Cycles.," *Energy*, vol. 35, pp. 1033-9, 2010.
- [38] M. E. P. A., "Efficiency prediction for axial-flow turbines operating with non conventional fluids.," *Transaction of ASME, Journal of Engineering for Power*, vol. 103, pp. 718-24, 1981.

- [39] E. D. o. E. -. P. d. M. Macchi, "The choice of the working fluid: The most important step for a successful ORC (and an efficient turbine)," 2013. [Online]. Available: <http://asme-orc2013.fyper.com/uploads/File/ORC2013%20-%20Kenynote%20lecture%20Prof.%20Macchi.pdf>. [Accessed 12 11 2018].
- [40] C. R. T. M. S. T. Sanchez D, "Stirling based fuel cell hybrid systems: an alternative for molten carbonate fuel cells," *Power Sources*, vol. 192, pp. 84-83, 2008.
- [41] W. C. ., C. W. ., Y. L. Yin Hai Zhu, "Fuel ejector design and simulation model for anodic recirculation SOFC system," *Journal of Power Sources*, vol. 173, pp. 437 - 449, 2007.
- [42] W. C. Y. L. C. Yin Hai Zhua, "Anode gas recirculation behavior of a fuel ejector in hybrid solid oxide fuel cell systems: Performance evaluation in three operational modes," *Journal of Power Sources*, vol. 185, pp. 1122-1130, 2008.
- [43] J. C. C. W. V. P. B.J. Huang, "A 1-D analysis of ejector performance," *Int. Journal of Refrigeration*, no. 22, pp. 354-364, 1999.
- [44] A. L. W. H. V. C. A. V. P. A. Ming Liu, "Anode recirculation behavior of a solid oxide fuel cell system: A safety analysis and a performance optimization," *International Journal of Hydrogen Energy*, no. 38, pp. 2868 - 2883, 2013.
- [45] D. C. LJ, "Combined numerical/analytical perturbation solutions of the NaviereStokes equations for aerodynamic ejector/mixer nozzle flows.," *NASA/CR*, 1998.
- [46] B. N. S. P. W. S. B. S. C. W. B. G. Lee SMITH, "25kW low-temperature Stirling Engine for Heat Recovery, Solar, and Biomass Applications," 16 1 2017. [Online]. Available: https://www.ohio.edu/mechanical/stirling/ISEC_2016_papers/ISEC2016-CoolEnergy.pdf. [Accessed 2 10 2018].